Carbon Black Nanofluid Synthesis for the Use in Concentrated Solar Power Applications

JJG Bester

15/11/2016

UNIVERSITEIT VAN PRETORIA
UNIVERSITY OF PRETORIA
YUNIBESITHI YA PRETORIA

Carbon Black Nanofluid Synthesis for the Use in Concentrated Solar Power Applications

Dissertation submitted in partial fulfilment of the requirements for the degree Masters in Engineering

JJG Bester
11035103

Department of Chemical Engineering
University of Pretoria

15/11/2016

Carbon Black Nanofluid Synthesis for the Use in Concentrated Solar Power Applications

Synopsis

Direct absorption solar collectors offer possible improvement in efficiency over traditional surface absorbing collectors, because they have fewer heat transfer steps and has the ability to utilise higher radiation fluxes. Carbon black based nanofluids, in a base fluid of salt water, were synthesised by a two-step method where the carbon black nanoparticles were treated with a surfactant, TWEEN-20, in a 1:2 mass ratio and sonicated for 60 minutes to break up agglomerates. The synthesised nanofluids showed stability for over 31 days. The different carbon black concentration nanofluids' solar irradiation absorption properties were compared with each other and with the base fluid of salt water in a concentrating, as well as non-concentration scenario. It was found that the carbon black nanofluids showed excellent absorption properties over the entire solar radiation spectrum. A 1 m^2 concentrating unit using a two-axis tracking system, with two mirrors and a 1 m diameter circular Fresnel lens, was used to concentrate solar radiation on a direct absorption solar collector flow cell with a 10 cm^2 collection area. An optimum concentration of 0.001 volume % carbon black was found to show a 42 % increase in heating rate, compared to that of salt water. The collector was, however, hampered by high energy losses and the maximum collector efficiency achieved was only 46 %, 23 % higher than that of salt water. The overall system efficiency was only 22 %. This low efficiency can be attributed to the high optical concentration losses (50 % − 70 %) present in the concentrating unit.

KEYWORDS: nanofluid; carbon black; concentrated solar power; direct absorption solar collector.

Contents

List of Figures

List of Tables

1. Introduction

Solar energy supports all life on earth in a variety of ways, with the most predominant being photosynthesis. The solar resource however, is still extremely underutilised in a synthetic fashion. The largest advantage that solar energy offers is a 'free' energy source that is both renewable and non-polluting (Tyagi et al., 2009, Yu and Xie, 2012). In the past fossil fuels have been used as primary energy source because of its reliability and inexpensive nature. The environmental impact of this fuel source has been largely ignored until recent years. The current trend is more towards developing and using alternative energy sources, especially renewable sources of which solar energy shows great promise (Kalogirou, 2004). South Africa has very high solar radiation levels compared to the world averages. This makes developing technologies utilising the abundant solar energy in South Africa all the more relevant.

Water scarcity is one of the biggest problems the world is facing. Dwindling clean water sources, as a result of drought, pollution and ever increasing demand has made it a necessity to find alternative water sources. Sea water has the biggest potential as a largely untapped, clean water source (Sharon and Reddy, 2015). Sea water desalination however, is one of the most expensive ways to produce potable water. This is due to the high capital costs and the high salinity content resulting in high energy costs (Li et al., 2013). South Africa is currently in the midst of a water crisis combined with an energy crisis. This is driving the need for the development of solar assisted desalination technologies.

Concentrated solar power (CSP) offers some advantages over non-concentrating systems. The two most significant advantages being smaller collection areas, which relate to smaller heat loss areas, especially infrared losses, and 'higher-quality' energy that relate to higher temperatures that can be reached. This higher

temperature results in a higher temperature difference over the energy collection surface area and therefore higher thermodynamic efficiencies are possible (Zarza and Romero-Alvarez, 2007, p. 21-6). It does however, come at the cost of additional optical losses, energy spillage (only the direct normal irradiance (DNI)) fraction of the solar radiation is utilised and a form of tracking system is necessary which increases the capital expense (Kalogirou, 2004).

Solar collectors are devices which absorb sunlight and convert it to thermal energy. Generally solar collectors are surface collectors absorbing the solar radiation on a flat plate and transferring the thermal energy through conduction to a working fluid. This type of collector has numerous thermally resistive steps and is limited not only by the efficiency of solar irradiation absorption, but also the efficiency of the heat transfer from the heated surface to the working fluid (Otanicar et al., 2010a). In comparison, volumetric absorbers or direct absorption solar collectors (DASC) absorb the solar radiation directly in the working fluid, thereby heating the fluid directly. This reduces the thermal resistance network, leading to higher efficiencies when the working fluid is chosen correctly. Such a collector is also able to utilise higher incident fluxes making it an ideal technology to use with CSP (Taylor et al., 2011b, Tyagi et al., 2009).

The term 'nanofluid' describes a system where nanoparticles are added to a base fluid to create a colloidal suspension (Ghadimi et al., 2011). Because there are a vast number of different types of nanoparticles, all with different material properties, it is possible for a nanofluid to be engineered for a specific purpose. This makes nanofluids ideal working fluids in DASCs. Carbon based nanofluids have excellent absorption properties across the entire solar radiation wavelength range (Otanicar et al., 2010b, Han et al., 2011, Sani et al., 2011). Carbon black nanoparticles are produced by the incomplete combustion of hydrocarbon precursors. This controlled reaction is very simple, making carbon black

inexpensive to manufacture (Pierson, 1993), which qualifies carbon black based nanofluids as one of the cheapest available carbon based nanofluids.

In the last few years there has been an extensive amount of research done on nanofluids and a large number of the studies on the solar energy applications of nanofluids. Very little research has of yet been dedicated to nanofluids implemented in concentrated solar power applications. The studies that looked at high intensity irradiation of nanofluids focused on the behaviour of stagnant nanofluids where the only movement of the nanoparticles is a result of Brownian motion and buoyancy driven flow. There hasn't yet been much consideration given to the behaviour of a flowing nanofluid in a concentrated solar power application theoretically or experimentally.

The objective of this investigation was firstly to synthesise a stable carbon black nanofluid in a base fluid of salt water and characterise the solar irradiation absorption properties. Secondly, it was necessary to get an understanding of how the nanofluid interacts in a flowing system with concentrated solar radiation and quantify the improvement on performance offered by a nanofluid. This would serve as the first step towards a solar desalination system using concentrated solar power as well as fill a lack of experimental data for a flowing nanofluid in a concentrated solar power application.

The carbon black nanofluid will consist of carbon black nanoparticles suspended in simulated sea water. The nanofluid will be characterised in terms of its absorption properties and photothermal properties for different concentrations of carbon black. From this information, a DASC will be designed and manufactured. The experiments will be done on a pilot scale solar concentrating unit, concentrating 1 m^2 of solar radiation. This pilot scale setup is located on the

experimental farm at the University of Pretoria in South Africa. The efficiency of the collector, as well as the system will be determined on this setup.

The chapters to follow start with a chapter to give a more in-depth background around the use of solar power and the need for desalination. The chapter also includes a literature survey on the latest research regarding the preparation, advantages and applications of nanofluids. The literature survey chapter is followed by an in-depth description of the experimental setups used, as well as the objective and short comings of each experiment. The experiments are categorised into two main sections, the first of which is regarding the characterisation of the nanoparticles and nanofluid. The second handles the application based experiments and the nanofluids' behaviour under concentrated solar irradiation. The results, as well as a discussion of the results, which derived from the described experimental setups are provided in the following chapter. This chapter is succeeded by a summary of the main conclusions that were drawn in the results chapter. The dissertation is finalised with a chapter of recommendation for future work to support the findings in this report.

2. Literature Survey

2.1. Renewable energy

Global energy needs are primarily satisfied by fossil fuels and while the energy demand is ever increasing, the fossil fuel sources are being depleted faster than nature can replenish them. In the past the easiest to reach fossil fuel resources have been tapped. Lately it has become necessary to extract the harder to reach, therefore more expensive, fossil fuel resources to satisfy the energy demands (Ladjevardi et al., 2013). The dwindling fossil fuel sources in combination, or rather especially, with the effect of climate change due to the high emissions from human activities, deem alternative renewable energy sources essential.

2.1.1. Solar irradiation as energy source

Several renewable energy sources are available and widely in use on different scales. Of these sources, solar energy shows a lot of promise because of its abundance and its non-polluting nature (Kalogirou, 2004, Tyagi et al., 2009). The biggest problem with the use of solar energy is its intermittency, which relates to the problems of inefficient utilisation and storage of solar energy.

2.1.2. Solar radiation components

Solar radiation is a form of electromagnetic energy transmitted through space in the form of photons. Only a small fraction of this energy reaches the earth's atmosphere and it has been found that the amount of energy reaching earth's atmosphere is relatively constant across the globe (Dekker et al., 2012). This value is expressed as the 'solar constant' and has a value of 1366.1 W/m^2 (ASTM, 2006). The solar energy reaching the earth's atmosphere is subjected to further losses

before it reaches the earth's surface where it can be captured and utilised. There are many factors affecting the amount of solar radiation reaching the earth's surface at a specific location. The main influences include: reflective losses from the atmosphere (albedo effect), absorption from particles and molecules in the atmosphere (ozone, water vapour and pollution) and the solar zenith angle (day of year, time of day, location and altitude) (Dekker et al., 2012, Ogunjobi et al., 2004).

The solar radiation reaching the earth's surface can further be classified into three categories based on the incident angle at which it reaches the earth's surface. The categories include: global horizontal irradiance (GHI), direct normal irradiance (DNI) and diffused horizontal irradiance (DHI). The DNI component of the solar radiation is defined as the fraction of solar radiation that comes in a straight line from the sun hitting the surface of the earth perpendicularly. Likewise, the DHI component of the solar radiation is defined as the fraction of the solar radiation that is scattered by various molecules and particles in the earth's atmosphere and does not reach the earth's surface at a right angle. The GHI is defined as the total amount of shortwave radiation on a horizontal surface to the earth's surface. Therefore the GHI is the combination of the DNI and DHI according to Equation 1 (Dekker et al., 2012).

$$GHI = DNI \cos\theta + DHI \tag{1}$$

With θ the zenith angle.

2.1.3. Solar radiation spectrum

The solar radiation reaching the earth's atmosphere is broken into separate wavelength ranges and each wavelength range's energy contribution to the solar energy is shown in Table 2.1 for a zero air-mass ratio (above the atmosphere) as

well as at a 1.5 air-mass ratio, which is a representation of the energy distribution at the earth's surface (ASTM, 2012).

Table 2.1: Solar radiation wavelength ranges and their contributions to the solar energy (ASTM, 2012).

Range name	Wavelength range (nm)	Portion of solar radiation (%)	
		Above atmosphere (Zero air-mass ratio)	At earth's surface (1.5 air-mass ratio)
UV-B	280 - 315	2.53	0.08
UV-A	315 - 400	12.57	6.75
Visible	400 - 800	48.51	53.87
Infrared	>800	36.39	39.30

When the solar radiation travels through earth's atmosphere it interacts with the particles and molecules present by being absorbed, reflected or refracted. This results in inevitable losses across the entire wavelength range of the solar radiation. A portion of the solar radiation is absorbed in the atmosphere, another part is reflected and scattered back into space (the albedo effect). In Table 2.1 it can be seen that the biggest loss of solar radiation energy is in the UV range. This is because of the ozone particles in the atmosphere absorbing the very short wavelength radiation. The largest fraction of energy reaching earth's surface is in the visible range. The fraction of infrared light reaching earth's surface is very dependent on the amount of water vapour in the air, as water is an excellent absorber of the long wavelength radiation. The amount of water in the atmosphere varies by time of day, location, season and lots of other meteorological occurrences. Therefore, the breakdown of the different wavelength range contributions is merely an indication as per the ASTM standards.

2.1.4. Solar irradiation in South Africa

South Africa has an above global average solar resource, especially in the Northern Cape region (Le Roux, 2016), as can be seen in Figure 2.1. This makes finding more efficient solar energy applications very relevant in South Africa.

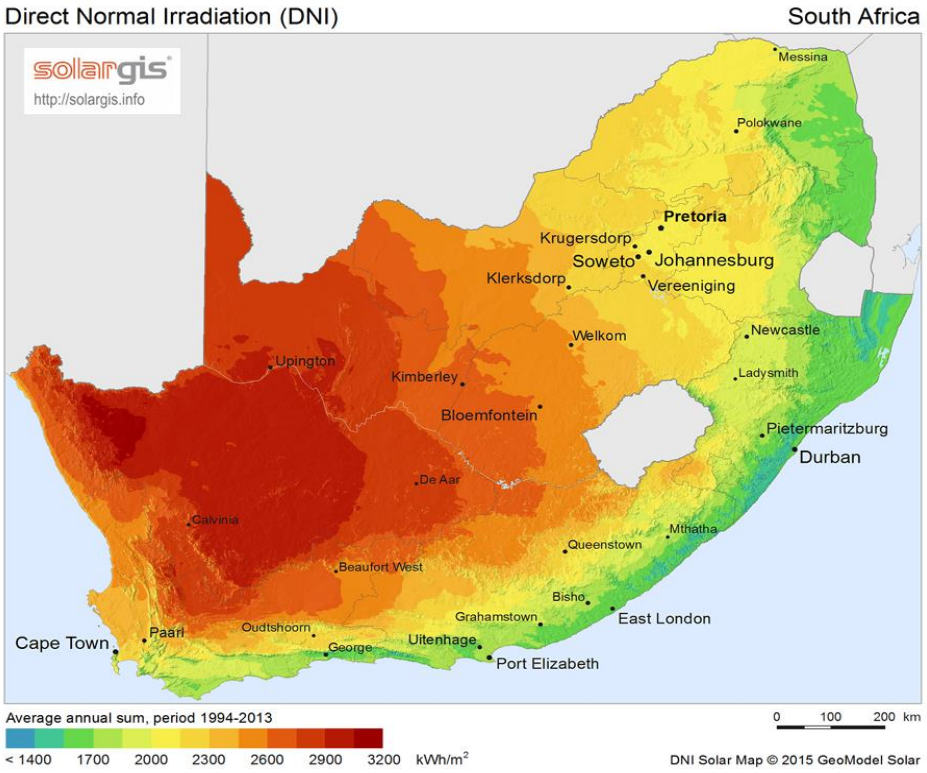

Figure 2.1: Solar irradiation map of DNI in South Africa. (SolarGIS © 2015 GeoModel Solar)

2.1.5. Solar utilisation methods

Solar energy can be utilised in two main methods: photovoltaic (PV) systems and thermal systems. In PV systems, the solar energy is converted to electricity by utilising the photovoltaic effect in semi-conducting materials where an electron is released upon excitation by photons. Solar PV systems are limited by the fact that they only absorb a small fraction of the solar irradiance spectrum and lose a lot of efficiency at elevated temperatures. Solar thermal systems on the other hand,

absorb the solar irradiation and convert the light energy to heat. The heat can then be used in several different applications (Saroha et al., 2015, Ladjevardi et al., 2013).

2.1.6. Concentrated solar power

Concentrated solar power (CSP) technologies have received a lot of attention in recent years, regarding both concentrated photovoltaics (CPV) as well as thermal systems. In CSP systems, optical equipment (mirrors or highly reflective metals) is used to focus the DNI component of the solar irradiation on a small surface. This increases the intensity of the solar radiation because it is focused on a smaller surface. It does however, not change the amount of energy available in the system. The optical reflective systems are combined with a solar tracking system to follow the sun's trajectory and thereby maintain optimal efficiencies. The four main CSP technologies available are parabolic trough collectors (PTC), linear fresnel reflectors, parabolic dish systems and central tower systems (Ghaffour et al., 2015). The different systems are schematically represented in Figure 2.2. PTC is the most mature CSP technology, but in recent years there have been several megawatt-scale central tower systems built. Linear fresnel reflectors show easier operability and maintainability, because of its modular reflection system, in comparison to PTC systems.

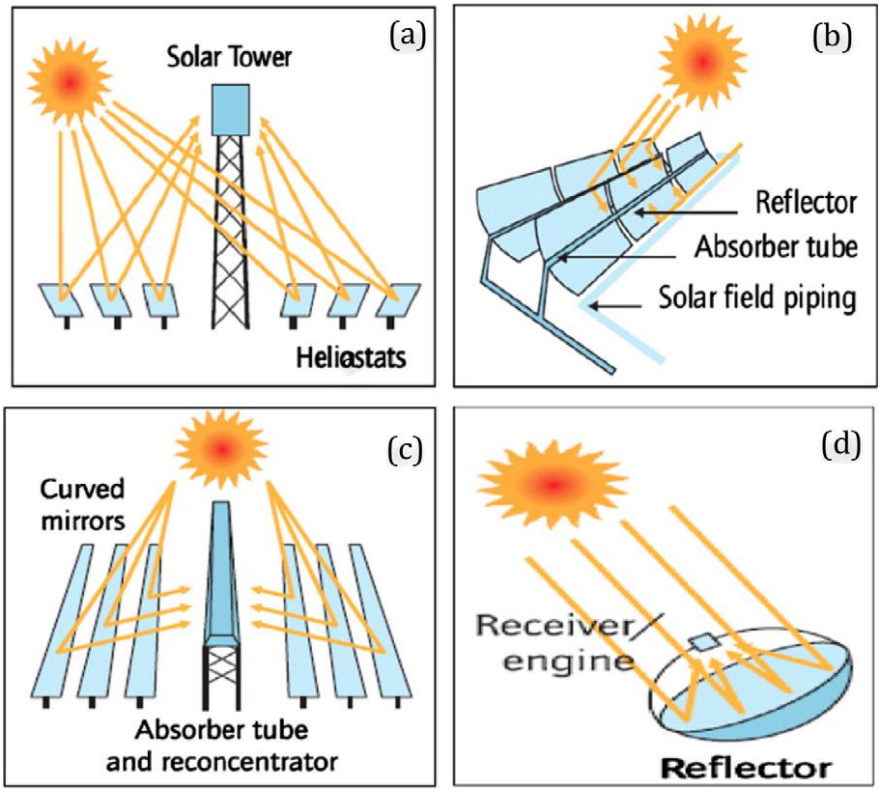

Figure 2.2: CSP technologies schematic representations (Ghaffour et al., 2015).

Concentrated systems offer some advantages over non-concentrating systems. The two largest being smaller collection areas, that relate to smaller heat loss areas, especially infrared losses, and 'higher-quality' or more intense energy that relate to higher temperatures that can be reached. This higher temperature results in a higher temperature difference over the energy collection surface area and therefore higher thermodynamic efficiencies are possible (Zarza and Romero-Alvarez, 2007, p. 21-6). The concentration process does, however, have some distinct disadvantages: inherently all concentrating systems have energy losses in the optical concentration steps, how significant these losses are, is dependent on the concentration setup, the nature and accuracy of the solar tracking system as well as the reflecting surface material's quality and cleanliness. Another big downside of using CSP is that, due to the angle at which the different components of the solar irradiation hits the reflecting surface, only the DNI fraction of the solar radiation is utilised leading to 'energy spillage' of the additional DHI component, which is not insignificant (Zarza and Romero-Alvarez, 2007, p. 21-29). With the optical energy

losses and additional energy spillage, the biggest deterrent from using CSP systems is the very large capital expense for the concentration setup (Kalogirou, 2004). The success of using CSP will therefore be dependent on the trade-off between the collector efficiency and the optical losses. The applicability of CSP will be determined by weighing the improved efficiency against the additional capital costs.

2.2. Desalination

Similar to the world's energy demands, the world's fresh water demands are also increasing drastically. Dwindling fresh water supplies is a major concern and the forecasts from the World Health Organisation and similar entities look extremely grim in terms of fresh water availability (Sharon and Reddy, 2015). It is therefore essential that alternative fresh water sources are found. One of the largest alternative fresh water sources is desalinated sea water. Desalination of sea water is very energy intensive, and therefore expensive, because of the high salinity content of the water (Li et al., 2013, Ghaffour et al., 2015). The high energy demands are mostly satisfied by fossil fuel resources, contributing to the energy crisis and leading to an even larger water crisis. Therefore, in order to sustainably produce fresh water from sea water, renewable energy sources have to be used to drive the desalination.

Because of this driving force, a lot of research on renewable energy coupled desalination technologies has been done. There are also several pilot scale desalination plants and, although less common, some industrial scale plants are already operational. All forms of renewable energy can be used to satisfy the energy needs of desalination, but the majority of active plants use solar energy (Sharon and Reddy, 2015). This is mainly because the countries that have

implemented the systems are located in the Middle East where solar energy is abundant.

CSP can be used in several ways to drive solar assisted desalination. Concentrated PV systems have been receiving lots of attention and can deliver the electricity demands for existing desalination technologies. The thermal energy can be used directly as well, by heating a working fluid or salt, to drive a secondary evaporation loop to desalinate the water. It is also possible to use the saline water as working fluid, especially if solar irradiation absorption can be sufficiently improved. This system will also harness the solar thermal energy of the sun. The biggest problems facing solar assisted desalination technologies are the intermittency and unreliability of the solar resource. To mitigate these problems solar thermal systems have the added benefit of solar storage solutions (e.g. phase change materials) for longer operational hours in a day, as well as the easy ability to use a backup energy source in unexpected conditions. (Li et al., 2013).

2.3. Direct absorption solar collector

A solar collector is a device that uses solar thermal energy by absorbing incident solar radiation and converting it to heat (Kasaeian et al., 2015). There are two types of solar collectors: surface and volumetric absorbers. A surface solar collector absorbs the solar radiation on a surface (usually coated with a selective absorber), heating the surface and the surface subsequently heats a working fluid. This type of collector's efficiency is therefore limited not only by the solar irradiation absorption efficiency, but also by the efficiency of the heat transfer between the surface and the working fluid (Otanicar et al., 2010b). In a volumetric absorber solar collector or a direct absorption solar collector (DASC), the solar irradiation is directly absorbed in the working fluid. This reduces the number of steps in the heat resistance network and therefore results in a more efficient system

being possible. The efficiency of a volumetric absorber is however directly dependent on the solar irradiation absorption properties of the working fluid (Taylor et al., 2011b, Ladjevardi et al., 2013, Saroha et al., 2015).

2.4. Nanofluids

Nanoparticles are defined as particles with a dimension in the 1 nm – 100 nm range (Fendler, 2001). The term 'nanofluid' describes a system where nanoparticles are added to a base fluid to create a colloidal suspension (Ghadimi et al., 2011). Because there are a vast number of different types of nanoparticles, all with different material properties, it is possible for a nanofluid to be engineered for a specific purpose by merely changing the type of nanoparticles used (Gupta et al., 2012).

Millimetre and micrometre sized particles added to a base fluid are known to improve the thermal conductivity of the fluid, but their applications are limited by their instability that leads to sedimentation, mainly because of size effects. Nanoparticles show better stability in fluids because of their smaller size and increased Brownian motion of the nanoparticles in the fluid. (Li et al., 2009)

A lot of research has been done to improve specific properties of nanofluids with the majority of research focused on improving the thermal conductivity of working fluids in heat transfer systems (Li et al., 2009, Choi et al., 2008, Taylor et al., 2013). Lately, a lot of research around the optical properties of nanofluids has been done with nanofluids being extensively researched specifically for the use in DASCs (Taylor et al., 2013).

Solar collectors' efficiencies are limited by low solar radiation absorption and low thermal conductivities of conventional working fluids (Goudarzi et al., 2015).

Various metals have been researched, predominantly for the purpose of improving the thermal conductivity of heat exchange fluids (Gupta et al., 2012), but research has been done with multi-wall carbon nanotubes (MWNT) (Yousefi et al., 2012, Hordy et al., 2014), single-wall carbon nanohorns (SWCNH) (Sani et al., 2011, Moradi et al., 2015, Mercatelli et al., 2011), graphite (Ladjevardi et al., 2013, Otanicar et al., 2010b), graphene (Liu et al., 2015) and carbon black (Sani et al., 2011, Hwang et al., 2008, Han et al., 2011).

From the fluids typically employed as heat exchange fluids in solar collectors, water shows the highest solar radiation absorption at only 13 % (Otanicar et al., 2009). Compared to water, all nanofluids have shown a significant improvement in the absorption of solar irradiation (Zhang et al., 2014). Carbon based nanofluids have excellent photo-thermal properties with graphite nanoparticles in water as base fluid found to absorb 96 % of solar radiation (Otanicar et al., 2010b) and SWCNHs found to absorb 95 % (Mercatelli et al., 2011). This shows the possibilities in improving the efficiency of DASCs using carbon based nanofluids.

2.4.1. Nanofluid stability

The biggest limitation to using nanofluids in any application is the stability of the nanoparticles in the fluid (Hordy et al., 2014, Gupta et al., 2012). Nanoparticles have a very high surface area to volume ratio that relates to a high surface energy and strong van der Waals forces acting between the particles attracting each other. This results in a tendency to agglomerate and lower the surface energy of the particles (Ghadimi et al., 2011). The agglomerated particles have larger sizes that increase the settling rate and decrease the stability of the nanofluid. In previous studies, nanofluids are characterised as stable without a standardised definition of stability (Hordy et al., 2014). Therefore, a 'stable nanofluid' in this study is

described as the negligible settling of nanoparticles from the base fluid that does not negatively affect the efficiency of the system.

There are generally three principles to increase the stability of a nanofluid: Electrostatically, by changing the zeta potential of the colloidal suspension, thereby increasing the repulsion forces between particles (Fendler, 2001, Ghadimi et al., 2011). Sterically, by increasing the steric hindrance in the adsorption layer of the particles (Fendler, 2001), or by reducing the hydrophobic linkages between particles (Ghadimi et al., 2011), and thirdly, by breaking up the already formed agglomerates by applying an external force on the colloidal suspension. These methods have been used successfully for multiple nanofluid applications, individually or in a combination (Ghadimi et al., 2011). The three principles can be applied using the following methods:

2.4.1.1. Surfactant

The addition of a surfactant is one of the most used methods of stabilising a nanofluid. Absorbing surfactants onto the particles' surface changes the nature of the surface from hydrophobic to hydrophilic, or vice versa. The change in nature of the particle surface also increases the zeta potential and thereby increasing the electrostatic repulsion forces between suspended particles. Adding a surfactant stabilises a nanofluid both sterically and electrically (Fendler, 2001, Ghadimi et al., 2011). Water has a highly polar nature and therefore will need a bipolar additive or surface treatment for particles (Vander Wal et al., 2009).

The amount of surfactant also plays a role in the stability of a colloidal suspension. Too little surfactant leads to an inadequate surface coating on the particles and insufficient electrostatic repulsion forces between particles to overcome the van der Waals forces between particles (Ghadimi et al., 2011). On the other hand, too

much surfactant leads to micelle formation in the surfactants and flocculation because of bridging between the particles (Rastogi et al., 2008).

There is an extensive range of surfactants available. The best surfactant is dependent on the application and type of nanoparticles. The most used surfactant is sodium dodecyl sulfate (SDS). Oleic acid, TWEEN-20 and TWEEN-80 are also some of the more used surfactants. For carbon nanotubes, it was found that TWEEN (both 20 and 80) is a more effective dispersant than SDS in water (Rastogi et al., 2008).

2.4.1.2. pH control

Another method often employed to increase the stability of a colloidal suspension is to change the pH of the solution. The pH directly relates to the electro-kinetic properties of the fluid (Ghadimi et al., 2011) and therefore affects the stability of the colloidal suspension electrostatically. The isoelectric point (IEP) of a solution is the pH at which the solution carries no net charge (zeta potential is zero). As the pH of the solution moves further away from the IEP, the repulsion forces between particles get higher and this leads to a higher stability of the colloidal suspension (Ghadimi et al., 2011).

Pre-treatment of carbon nanotubes by acid also increases the stability of a carbon nanotube suspension by changing the surface nature of the carbon nanotubes from hydrophobic to hydrophilic, because of a hydroxyl group attaching on the surface (Xie et al., 2003).

2.4.1.3. Ultrasonication

The previous methods interact with the surface of the particles (sterically and electrically) in an attempt to avoid agglomeration. Ultrasonication is a method that uses intense sound energy to break up agglomerates that have already formed and

distributing the particles homogeneously (Ghadimi et al., 2011). Because of this, the method is most frequently employed in combination with the other methods (Taylor et al., 2013).

2.4.2. Nanofluid preparation

Nanofluid preparation techniques are classified into two categories: the single step and two-step methods (Ghadimi et al., 2011, Hwang et al., 2008, Li et al., 2009).

2.4.2.1. Single-step method

In the single-step method, the nanoparticle production as well as the nanofluid synthesis is done simultaneously. The nanoparticles are prepared using a physical vapour deposition technique after which the vapour phase particles are condensed into a moving fluid. By doing this, the agglomeration of nanoparticles is minimised because the drying, storage and transportation steps are avoided. This method is however limited to lab scale experiments and only possible for base fluids with a low vapour pressure. (Ghadimi et al., 2011, Taylor et al., 2013, Li et al., 2009, Yu and Xie, 2012, Hwang et al., 2008).

2.4.2.1.1. Two-step method

In the two-step method the nanoparticles are produced in a separate step after which they are dispersed into a base fluid to create a colloidal suspension. In the two-step method the stability is a larger problem than in the one-step method because of more agglomeration taking place in the extra synthetisation steps. The two-step method, however, is much less expensive because nanoparticle production has already been commercialised on an industrial scale. Therefore, the two-step method is by far the most frequently used method for the production of nanofluids. (Ghadimi et al., 2011, Yu and Xie, 2012, Taylor et al., 2013, Li et al., 2009, Hwang et al., 2008)

2.4.3. Carbon nanoparticles

There are various forms of carbon nanomaterials available e.g. cones, rods, tubes, fullerenes, horns, carbon black and more.

2.4.3.1. Production method

Carbon black nanoparticles are produced by the incomplete combustion of a hydrocarbon precursor such as methane, hydrocarbon oils or acetylene (Pierson, 1993). This controlled reaction is a very simple process and therefore it is very inexpensive to manufacture carbon black.

Carbon nanotubes and nanohorns can be manufactured in multiple ways, but the catalytic chemical vapour deposition (CVD) method is the preferred method (Paradise and Goswami, 2007, Pagura et al., 2010). Compared to the production process of carbon black, the CVD process is very complex and therefore more expensive.

2.4.3.2. Carbon black molecular structure

Carbon black is classified as an amorphous carbon that is not graphitisable. On a very small scale, however, it consists of sections of microcrystalline arrays of condensed rings, similar to graphite. The microcrystal orientation is random and results in a large fraction of crystal arrays that have unsatisfied carbon bonds at the end of their layer planes located at the surface of the amorphous particle. These unsatisfied bonds on the surface provide chemical active sites. (Norman, 2014)

2.4.3.3. Solar absorption property comparison of carbon nanoparticles

From the results of Mercatelli et al. (2011) and Otanicar et al. (2010b) it can be concluded that the solar absorption properties of carbon nanotubes and nanohorns are the same. It was however found that carbon nanohorns have better

solar absorption properties than carbon black (Sani et al., 2011) which is supported by (Wagner et al., 1980) that found the optical absorption of India inks (which is carbon-black based) to be 85 %. However, taking the economical factor into account, carbon black is a more suitable option for the wide spread use in solar collectors.

2.5. Literature summary

The solar radiation reaching the earth's surface is predominately in the visible wavelength range (400 nm – 800 nm) with approximately 54 % of the solar radiation falling in this range. The rest of the available solar radiation spectrum is in the infrared range, above 800 nm (approx. 39 %) and the UV range, below 400 nm (approx. 7 %). The solar radiation across all the applicable wavelength ranges reaching the earth's surface can subsequently be classified into different categories depending on the angle at which the solar radiation hits the earth's surface. The categories include GHI, DNI and DHI. CSP systems offer the advantage of smaller collection areas relating to smaller heat loss areas as well as a higher-quality energy for a collector. It does however, come at the cost of additional optical energy losses, energy spillage (only the DNI portion of the solar irradiation is utilised) and the additional capital cost of the concentrating platform. The applicability of using CSP is dependent on weighing the improvement in efficiency of the system against the additional capital expense.

With dwindling clean water sources, an alternative source is essential. Sea water desalination is arguably the best alternative source of clean water, but because of its high salinity content relating to high energy requirements for desalination, it remains very expensive amid the current energy crisis in South Africa. It is therefore necessary to develop renewable energy powered sea water desalination units.

DASCs absorb solar radiation directly in the working fluid, therefore its efficiency is limited only by the working fluids absorption efficiency. This attribute is the discerning factor from a surface collector that is limited not only by the absorption efficiency of the collecting surface, but also by the energy transfer between the collecting surface and the working fluid. DASCs therefore offer a possible improvement in efficiency compared to that of surface collectors, if the working fluid is chosen correctly. DASCs are also better at handling the high energy flux of CSP.

Nanofluids are ideal working fluids for DASCs because they can be engineered for a specific application. Nanofluids offer improvements in various properties of a base fluid depending on the type of nanoparticles and the volume fractions of the nanoparticles in the fluid. Nanofluids can be prepared using a one-step or two-step method. The one-step method, although it shows improved stability over the two-step method, is limited to small-scale, lab experiments. The two-step method consists of sourcing the nanoparticles commercially and suspending the particles in a secondary step into the bulk fluid. The biggest limitation to using nanofluids is the colloidal instability of the fluid, with nanoparticles tending to settle out of the bulk fluid. The stability of nanofluids can be improved by various methods of which coating the nanoparticles with a surfactant and sonicating the fluid to break up the agglomerates, are the most cost effective and most widely used. Carbon-based nanoparticles have excellent solar irradiation absorption capabilities across the entire solar radiation spectrum. Of the various different types of carbon-based nanoparticles, carbon black is the simplest and cheapest to manufacture.

It is deduced from the literature that an investigation into a CSP powered desalination system using a DASC with carbon black nanoparticles suspended in salt water as the working fluid is warranted.

3. Experimental Method

3.1. Nanofluid preparation

The carbon black based nanofluid was prepared using the two-step method. Printex Degussa AG carbon black nanoparticles (approx. 80 nm) were suspended in a base fluid of simulated sea water. The simulated sea water is made up of 35 g/L of NaCl dissolved in tap water, as this is the approximate salinity of water around the Coast of South Africa (DWAF, 1996). The carbon black nanoparticles are coated with a non-ionic surfactant, TWEEN-20, in a 1:2 carbon black to surfactant mass ratio, prior to suspension in the base fluid. The colloidal suspension is sonicated for 60 minutes to break up agglomerates and obtain an evenly distributed solution. To consistently achieve the very low concentration nanofluids used in the study, a masterbatch solution was prepared in the above mentioned manner, then diluted with the base fluid. Figure 3.1 shows the carbon black concentration nanofluids used.

Figure 3.1: Carbon black nanofluids from left: 0.00; 0.0005; 0.001; 0.003, 0.005, 0.01, 0.05 volume % carbon black.

3.2. Particle characterisation

3.2.1. Scanning electron microscopy

Scanning electron microscope (SEM) images were obtained using an ultra-high resolution field-emission microscope (Zeiss Ultra Plus 55 FEGSEM) equipped with an in-lens detection system and operated at an acceleration voltage of 1 kV. A working distance of between 2 mm and 3 mm was used. The carbon black nanoparticles were lightly deposited on carbon tape and carbon coated.

3.2.2. Particle size analysis

The particle size of the carbon black particles in suspension was measured by using dynamic light scattering (DLS) principles with a Malvern Zetasizer Nano ZS.

3.3. Optical and thermal properties of nanofluid

3.3.1. Absorbance properties

The nanofluid's absorbance properties were determined by using an Apogee SP-100 spectroradiometer with range 350 nm to 1000 nm as constant receiver and a solar simulation light that has a similar radiation output as the sun as a constant light source. Figure 3.2 shows how the simulator light's output compares to that of the sun measured at the University of Pretoria on a cloudless day.

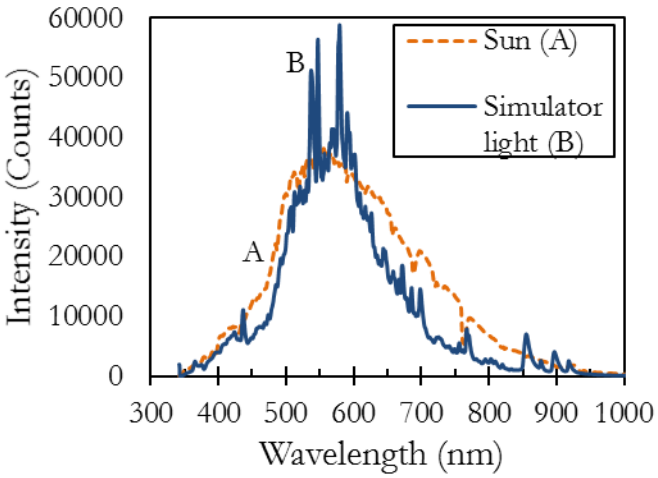

Figure 3.2: Comparison between solar spectrum and solar simulator light spectrum.

To determine a nanofluid's absorption properties a beaker was placed underneath the solar simulator light with the receiver at the bottom of the beaker. The nanofluid was added to the beaker using a 3 mL pipet and the light that was transmitted through the nanofluid and beaker was measured by the receiver. The transmitted light value was converted to an absorption value by subtracting transmitted light value from the incident flux value. A schematic diagram of the experimental setup can be seen in Figure 3.3.

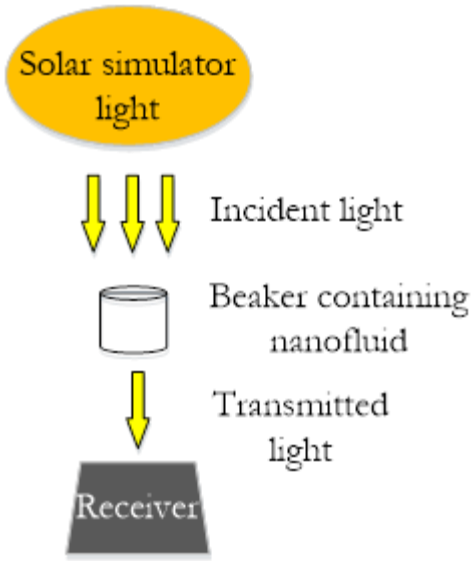

Figure 3.3: Schematic representation of the experimental setup to determine the absorption properties of fluids.

3.3.2. Extinction coefficients

The nanofluid's extinction coefficients and settling behaviour were measured using an Apogee SP-100 spectroradiometer with range 350 nm to 1000 nm as constant receiver and a 5 W LED light bulb as a constant light source. The LED light has an emission spectrum as shown in Figure 3.4. Two peaks are visible with the most intense, primary peak at 560 nm and the less intense, secondary peak at 458 nm.

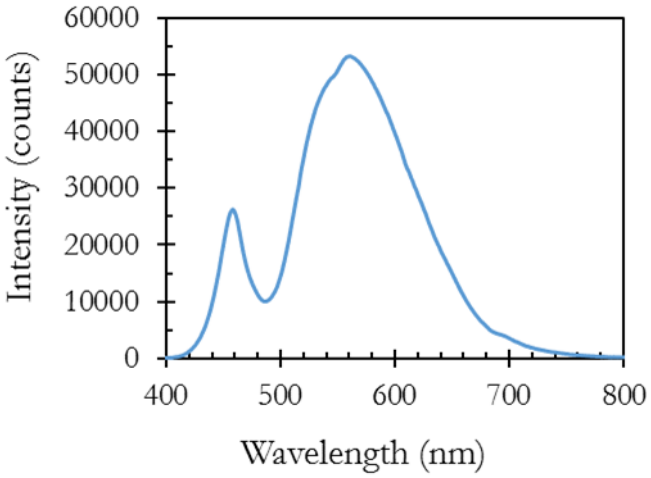

Figure 3.4: LED light transmission spectrum.

An experimental setup was designed and built to ensure a standardised experimental environment for the results to be comparable on consecutive days. The nanofluid was placed into a square polystyrene cuvette with a 1 cm path length. Reference measurements of the light were taken before, during and after sample measurements to ensure the light source, as well as receiver was constant. A schematic representation of the experimental setup can be seen in Figure 3.5.

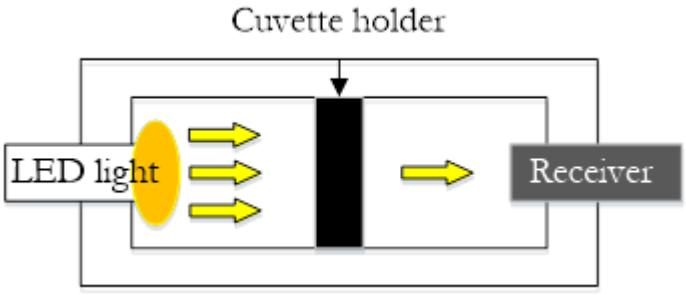

Figure 3.5: Schematic representation of the experimental setup to determine the extinction coefficient of a nanofluid.

3.3.3. Photothermal properties

The effect of carbon black concentration on the efficiency in which the nanofluid converts light energy to thermal energy was investigated by placing different concentrations of carbon black nanofluids into 50 mL polytop containers and placing a K-type thermocouple into the polytop to measure the temperature as a function of time. The polytop tubes were placed in insolating foam and placed in the sun on different days. Control samples of the base fluid were placed on each end to ascertain that the sample position did not influence the results. The experimental setup can be seen in Figure 3.6.

Figure 3.6: Photothermal property experimental setup.

3.4. Stability analysis

The time related stability of the nanofluids was primarily determined visually with the use of photographs taken over several weeks. The extinction coefficients experimental setup was used to determine the stability over a shorter time span. Particle size analysis, as described in the previous section, was also used to infer stability. The main goal of this experiment was to determine if the carbon black nanofluids will remain stable for at least a few days to be applicable for its intended use in the application of a flash desalination unit.

3.5. Concentrating platform

3.5.1. Description

The pilot scale concentrating platform consists of a primary mirror on a two-axis solar tracking system that reflects the solar irradiation onto a secondary mirror. From the secondary mirror the light is reflected through a circular Fresnel lens with a 1 m diameter. The operating principle of a circular Fresnel lens is shown in Figure 3.7 (Suman et al., 2015).

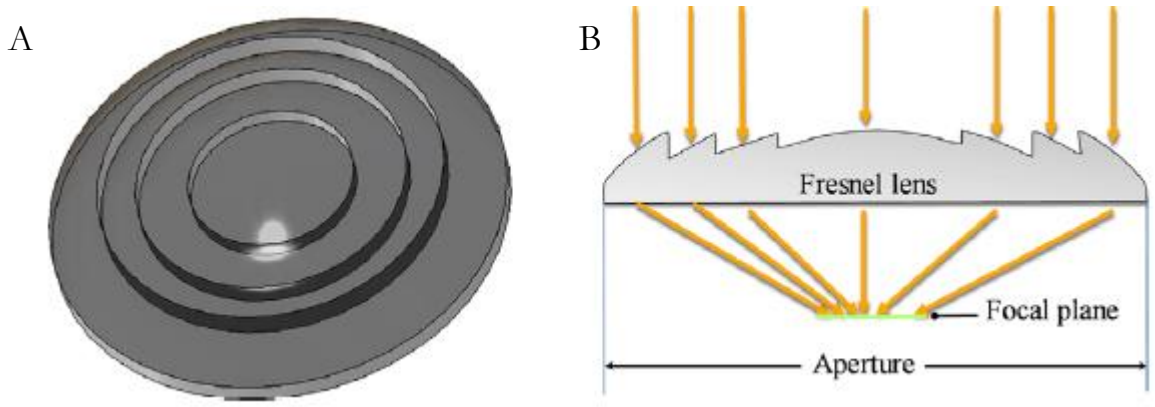

Figure 3.7: Circular Fresnel lens- A: design and B: operating principle. (Suman et al., 2015)

The concentrating platform operates essentially as a central tower system with only a single heliostat. Subsequently 1 m^2 of solar DNI is concentrated on a spot, with a 3 cm diameter at the focal point. This relates to a concentration ratio of approximately 1100. The focal length of the Fresnel lens is 130 cm. The system is shown in Figure 3.8.

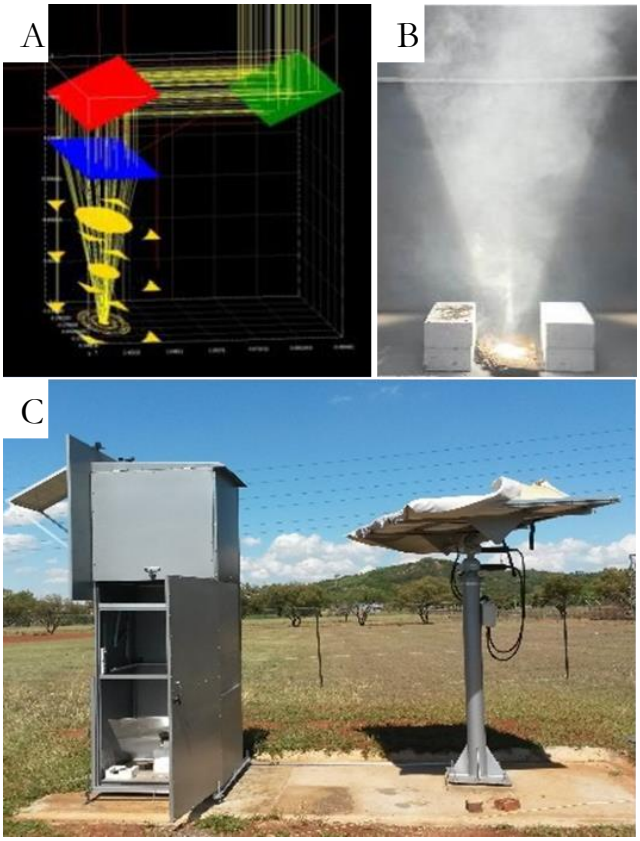

Figure 3.8: A: Representation of light travel path; B: Real representation of concentrated light beam and C: Concentrating platform

3.5.2. Characterisation

The system's energy losses were characterised using an Apogee MP-200 pyranometer. The MP-200 is a calibrated silicon-cell photodiode sensor with a manufacturer given accuracy of 5 % and a measurement range of 0 W/m^2 to 1500 W/m^2. The optical losses, occurring in the various concentration steps, were measured by taking energy readings after each optical step in the concentration process on multiple days, immediately after cleaning of the optical surfaces. The values were averaged to calculate the percentage optical losses in the system.

3.6. Concentrated solar radiation penetration depths

An experimental setup was designed to determine the approximate penetration depth of the concentrated solar beam into the carbon black nanofluids of different concentrations. An insulated foam container was made with six thermocouples spaced 15 mm from each other. The container has a depth of 105 mm and is open to the atmosphere on the top and enclosed with a perspex sheet at the bottom. The experiment was done at a concentration ratio of 100. A schematic representation of the experimental setup is shown in Figure 3.9. The nanofluid container is shown in Figure 3.10 A and B while in use. The concentration of nanofluids tested included 0.00 volume %, 0.0005 volume %, 0.001 volume %, 0.005 volume %, 0.01 volume %, 0.05 volume % carbon black nanofluid as shown in Figure 3.10 C.

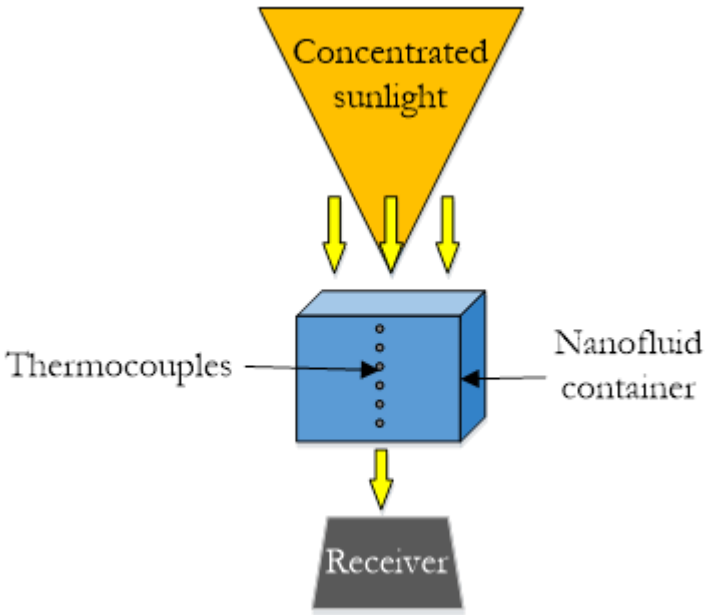

Figure 3.9: Schematic representation of the experimental setup to determine the solar radiation penetration depth into a nanofluid.

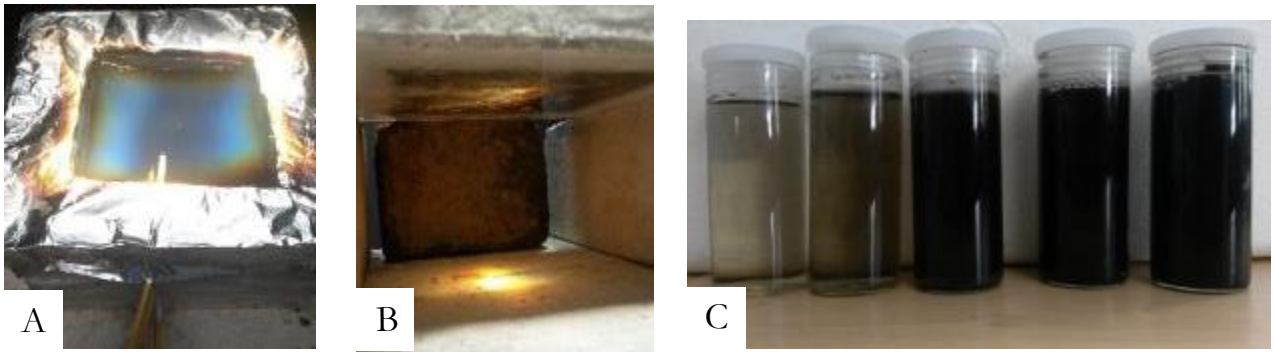

Figure 3.10: Absorption depth experimental container. A: top of container, B: bottom of container, C: nanofluid concentration range used.

3.7. Solar collector

A baffled flow cell was constructed from insulation foam and polycarbonate sheets. The collector has a collection area of 10 cm x 10 cm with 8 cm baffles spaced 1.5 cm apart to minimise the formation of dead spots in the flow path of the collector. Different design parameters were experimented with. The collector depth as well as the covering lid design was varied to determine the most efficient design. The collector depths investigated were 2.5 cm and 5 cm deep. The lid designs investigated were a single-pane, which consisted of a single 3 mm thick polycarbonate sheet, as well as a double-pane design, which consisted of two 3 mm thick polycarbonate sheets spaced 3 mm apart to reduce convective losses from the system. The outside walls of the collector are covered by foil to shield the silicon, attaching the polycarbonate lid to the foam body of the collector, from the concentrated irradiation. The flow cell in operation can be seen in Figure 3.11.

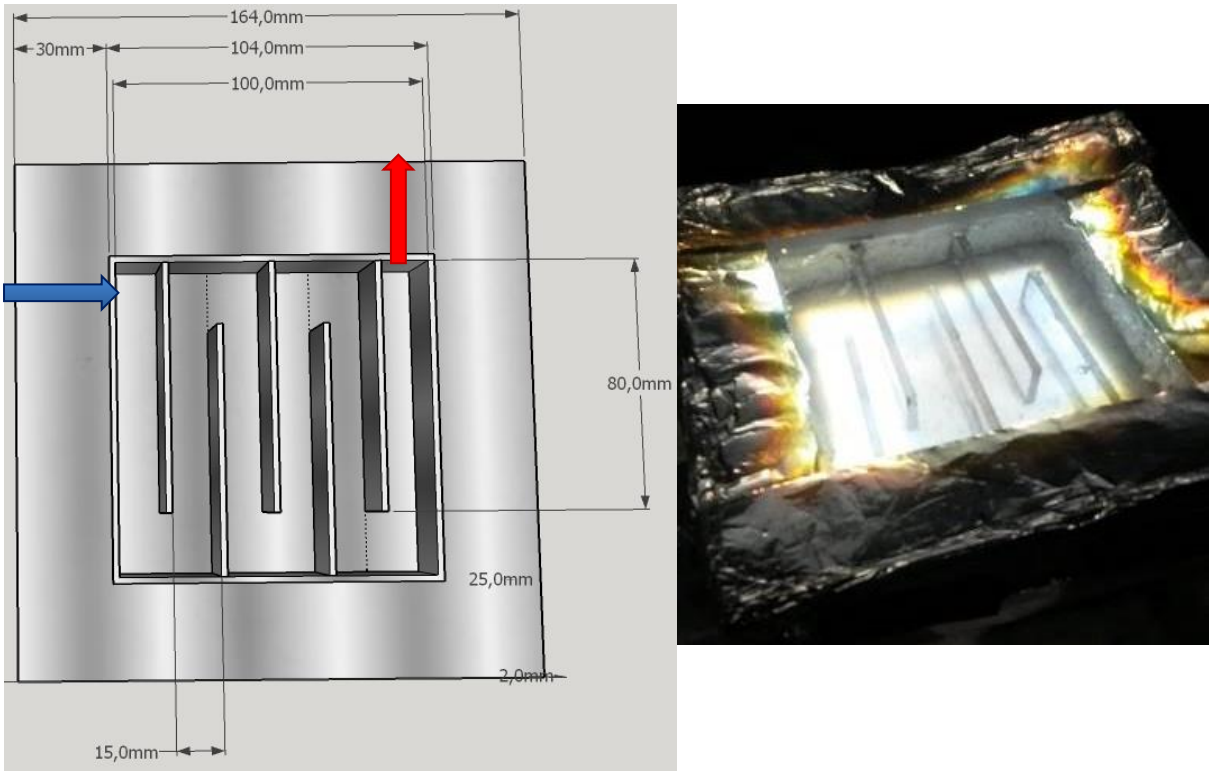

Figure 3.11: Solar collector flow cell.

3.8. Heating rate experiments

The heating rate behaviour of different carbon black concentration nanofluids were investigated by placing K-type thermocouples at both the inlet and outlet of the solar collector. The experiments were conducted over the course of a day and the temperature increase results were normalised by dividing the minute averaged temperature data with the minute averaged solar radiation data from the Southern African Universities Radiometric Network (SAURAN) database taken at the UPR - GIZ University of Pretoria station (Brooks et al., 2015), to make the data comparable. The behaviour of a stagnant carbon black-based nanofluid to show immediate nucleate boiling upon exposure to concentrated irradiation complicated the experimental setup to compare the heating rates of the nanofluids. This is due to the unaccountable losses present in the system when vapour is formed. If there is no lid to trap the vapour, the energy used for vaporisation is 'lost'. On the other hand, when a lid is used to trap the vapour in the system, the vapour condenses on

the surface of the lid, thereby increasing the scattering losses from the collector. This makes comparisons between experiments difficult. Therefore, to determine the heating rates of the nanofluids, it was necessary to have high enough flow through the collector to avoid immediate nucleate boiling, but low enough flow that a steady state system was not achieved (constant temperature difference over the collector). A steady state system was avoided because the aim of the experiment was to compare the unsteady heating-up process of the different nanofluids. A flow rate of 50 mL/min was used to characterise this nanofluid behaviour.

3.9. System efficiency experiments

The system efficiency (collector and overall) was investigated in a similar fashion to the heating rate experiments. Multiple K-type thermocouples were placed at the inlet, as well as the outlet of the solar collector. To be able to accurately determine the efficiency, a steady state system was necessary. Therefore, a flow rate that was high enough to assure a constant temperature difference over the solar collector was used. The system efficiency was determined for different flow rates, where the temperature difference over the collector remained constant for several minutes. A temperature measurement was taken every 6 seconds and it was averaged over a minute to compare the data to that of the radiation data from the SAURAN database (Brooks et al., 2015). The temperature difference, as well as the radiation data was averaged over the time for which the system had a constant temperature difference. The averaged data was used to calculate the collector and system efficiencies. The effect that carbon black concentration, flow rate and collector design parameters (collector depth and single or double-pane covering) had on the efficiency was investigated.

3.10. Applicability of using SAURAN solar radiation data

The UPR - GIZ University of Pretoria measurement station, where the solar radiation data for the SAURAN database is measured at the University of Pretoria, is positioned approximately 3 km away from the Experimental farm where the solar concentrating rig is positioned. It is therefore a pertinent concern whether the SAURAN database's solar radiation data is an accurate representation of the actual solar irradiation levels at the concentrating rig, as this value can significantly alter the efficiency calculations. To ascertain the applicability of the radiation data, measurements using the Apogee MP-200 pyranometer were taken on five cloudless days, at different times. This data was compared to the data from the SAURAN database for the relevant times. It was found that the data never varied more than 5 % from each other. Given the inevitable measurement uncertainties of 5 % for the Apogee MP-200 and additional measurement error (although this should be less than for the handheld pyranometer) in the SAURAN readings, it was concluded that the SAURAN database solar irradiation values were accurate enough to use for cloudless days.

4. Results and Discussion

4.1. Path to a stable nanofluid

Synthesising a 'stable' nanofluid was the most critical part of the study, because without a stable nanofluid no application would be possible. The final application is to utilise a DASC to do sea water desalination in a single heating loop. Therefore, the base fluid had to be salt water. For the study carbon black nanoparticles were chosen to be suspended in the base fluid because of their availability on a commercial scale and their inexpensiveness compared to other carbon based nanoparticles. The challenge was therefore to find a synthesis method to create a stable carbon black nanoparticle suspension in salt water.

4.1.1. Carbon black-salt water interaction

A trial-and-error approach was used to find a better understanding of how the carbon black nanoparticles interacted with the salt water base fluid. The initial experiments were done to understand the behaviour of the nanoparticles in suspension if no surface treatment were present. It was found that the untreated carbon black nanoparticles behaved in a very hydrophobic manner when added to the salt water. The carbon black nanoparticles would merely coalesce on the top surface of the water. Upon vigorous stirring for multiple minutes, a very unstable colloidal suspension would form where the nanoparticles formed immediate agglomerates that settled out of the bulk fluid within minutes. When the untreated carbon black nanoparticles were sonicated in the salt water, the agglomerates that formed were broken up and the colloidal suspension was stable for a few hours. However, when an external force was applied to the nanofluid, e.g. stirring or shaking, agglomeration of the carbon black nanoparticles started immediately. This led to the carbon black nanoparticles settling out of the bulk fluid in a similar

fashion as when no sonication was done. Thereby it was found, that some form of stabilisation method was essential to stabilise the colloidal suspension of carbon black in salt water.

4.1.2. Nanoparticle to surfactant ratio

Treating the carbon black nanoparticles with surfactant is the simplest method to improve the stability of the colloidal suspension. This stabilisation method is also very scalable, which is essential if the end objective of a commercialised desalination system is kept in mind. The addition of a surfactant stabilises the carbon nanoparticles in the salt water both sterically and electrically (Fendler, 2001, Ghadimi et al., 2011). A non-ionic surfactant polysorbate-20 (TWEEN-20) was chosen to be used because of its wide application in the food industry which supports the final application of producing drinking water. Rastogi et al. (2008) also found that TWEEN-20 is a more effective dispersant for carbon nanotubes than SDS, which is the most frequently used surfactant to stabilise nanofluids.

The ratio of carbon black nanoparticles to surfactant is an important variable in the stabilisation of a nanofluid. Different mass ratios of carbon black to TWEEN-20 were investigated. These ratios included: 1:0.5, 1:1, 1:2, 1:3, 1:5. For all of the ratios the carbon black was weighed and the relevant mass of TWEEN-20 was added to the carbon black nanoparticles. The mixture was stirred into a paste after which the salt water was added and the mixture shaken vigorously for a few minutes. It was found that the ratios 1:0.5 and 1:1 did not sufficiently cover the nanoparticles and resulted in uncoated carbon black nanoparticles that settled out within hours after suspension in the salt water. The higher ratios of 1:3 and 1:5 carbon black to TWEEN-20 showed a distinct, translucent TWEEN-20 micelle layer on the top surface of the nanofluid. The 1:5 ratio showed a thicker layer compared to that of the 1:3 ratio's layer, confirming that the phenomenon

occurred because of an excess amount of surfactant. This phenomenon was also described by Rastogi et al. (2008). The 1:2 ratio proved to be just right. All of the carbon black nanoparticles were covered by the TWEEN-20 and a thick paste was formed which, upon suspension in the salt water, remained stable for over a week. There was no layer separation visible in the 1:2 ratio of carbon black to TWEEN-20. Therefore, a mass ratio of 1:2 carbon black to TWEEN-20 was used in the following experiments.

4.2. Scanning electron microscopy (SEM)

SEM analysis was done on the carbon black particles as received from the supplier before undergoing any treatment. This was done to be able to discern between the inherent dimensional properties of the nanoparticles and the size effects due to the treatment and suspension of the particles in the base fluid. Subsequently, making it possible to better interpret the PSA experiments done on the synthesised nanofluid. The SEM micrographs are shown in Figure 4.1 at different levels of magnifications.

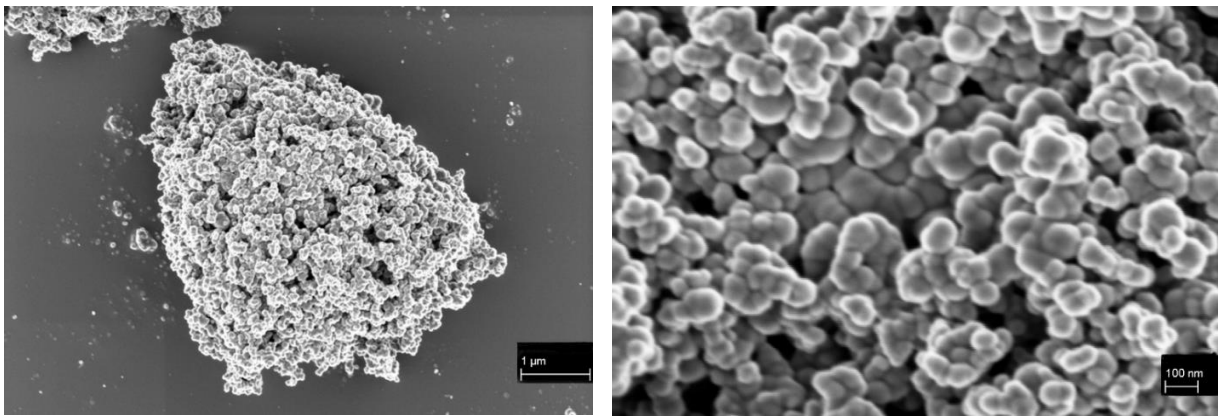

Figure 4.1: A: SEM micrograph of carbon black at 35 K magnification. B: SEM micrograph of carbon black at 160 K magnification.

From the SEM analysis it was found that there were small particles (< 100 nm) as well as larger particles (> 1 µm) present as can be seen in from Figure 4.1 A.

However, when the magnification on the large particles was increased, as seen in Figure 4.1 B, it is visible that the larger particles consist of smaller than 100 nm particles that have clumped together. This happens due to the strong intermolecular forces in relation to the size of the particles. The high surface energy of small particles is lowered by clumping together to form bigger agglomerated particles (Ghadimi et al., 2011). From Figure 4.1 B it is seen that the approximate average size of the carbon black spheres is 80 nm. Because of the nature of a SEM micrograph, which is the small fraction of the sample that is viewed, it is not necessarily an accurate representation of the bulk sample. The viewed particles are merely an indication that there are nanoparticles present in the sample and that they do tend to agglomerate.

4.3. Particle size analysis

The particle size distributions of the nanoparticles suspended in the synthesised nanofluids after sonication are shown in Figure 4.2. It can be seen that the suspended particles have sizes between approximately 90 nm and 900 nm, with an average hydrodynamic diameter of 250 nm. The larger particle sizes are due to agglomeration of particles that were most likely not wetted by the surfactant before being suspended in the base fluid. It can be seen that there are no significant differences between different concentrations of the carbon black nanofluids.

The solar spectrum reaching the earth's surface starts from a wavelength of 280 nm for the small fraction of UV-B light. This means that the majority of the suspended particles are smaller in size than even the shortest of wavelength of light reaching the nanofluid.

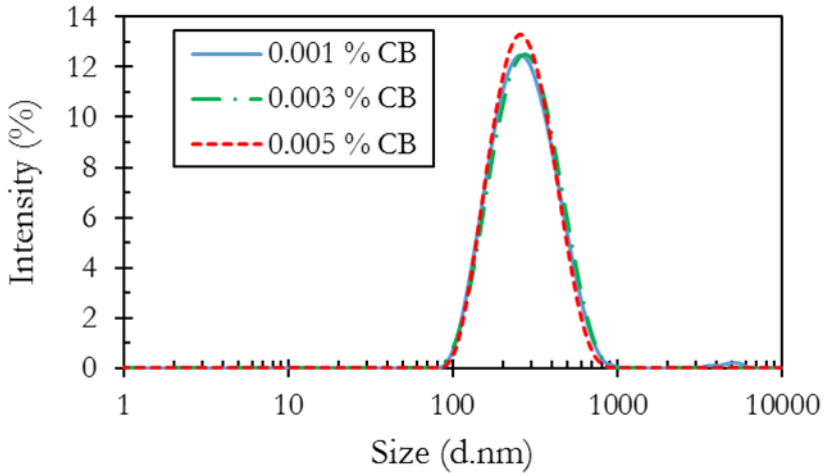

Figure 4.2: Particle size distribution for different carbon black (CB) concentration nanofluids.

4.4. Absorption properties

The absorption properties of the nanofluid play an important part in understanding the behaviour of the nanofluid and will affect the design of the solar collector. Using the experimental setup as shown in Figure 3.3, the absorption data for the different carbon black concentration nanofluids, shown in Figure 4.3 and Figure 4.4, are compared to that of the base fluid. It shows the increase in absorption of light compared to that of salt water.

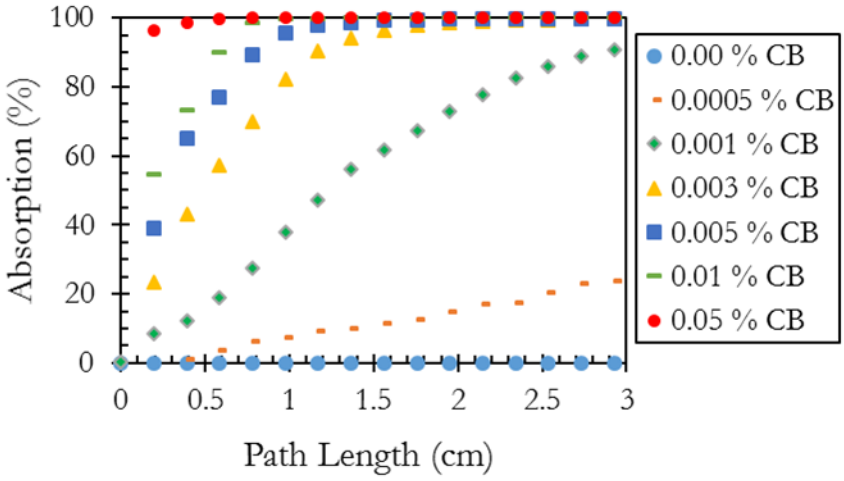

Figure 4.3: Absorption spectra for different concentrations of carbon black (CB) nanofluids with reference to base fluid immediately after synthesis.

From Figure 4.3 it can be seen that at very low concentration of 0.0005 vol % carbon black, the absorption of light increases linearly with the path length of the light following the Beer-Lambert law. At 0.001 vol % there is a tendency away from linearity and at higher concentration there is a very exponential trend visible between absorption and path length. At 0.05 vol % carbon black, an almost immediate complete absorption is visible. The experiment was done twice and a smaller than 2 % error between the readings was observed.

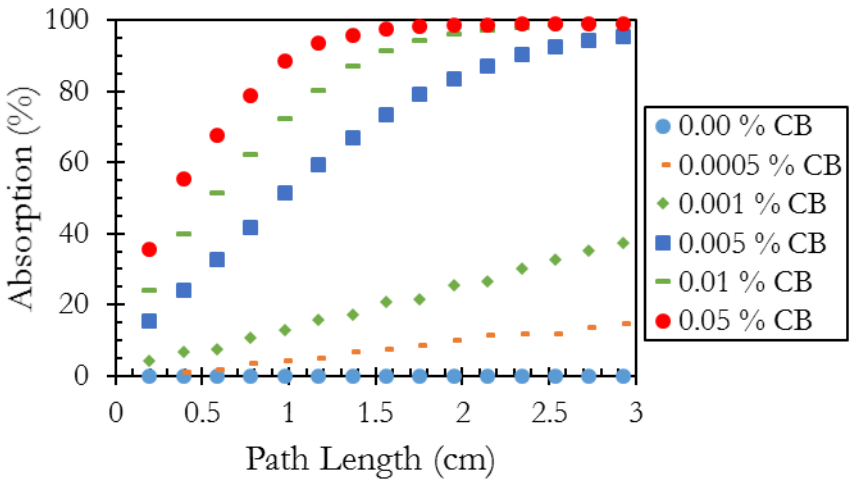

Figure 4.4: Absorption spectra for different concentrations of carbon black nanofluids with reference to base fluid after multiple heating cycles.

After one month and multiple heating cycles under concentrated solar power, the absorption properties of the nanofluids were tested again to compare with the nanofluid's properties immediately after synthesis, as shown in Figure 4.4. Comparing the absorption spectra of the different concentrations of carbon black nanofluid of the newly prepared and old, a trend is noticed where the higher carbon black concentration nanofluids of the old samples behave like the lower carbon black concentration nanofluids that were freshly prepared. Effectively, as the nanoparticles settle out of the bulk fluid, the concentration of nanoparticles suspended decreases, and the absorption properties of the nanofluid reflects that of a nanofluid with a lower carbon black concentration. It is seen that an 'old' 0.005 vol % carbon black nanofluid behaves like a new 0.001 vol % carbon black nanofluid. Similarly, an old 0.001 vol % carbon black nanofluid behaves likes a new 0.0005 vol % carbon black nanofluid. This effective concentration is dependent on all of the factors that influence the settling rate of the nanoparticles, which includes time, as well as the amount of heating cycles they have undergone.

It is apparent that the nanofluid does not fail catastrophically, where all the carbon black nanoparticles settle out simultaneously Rather, the nanofluid will lose absorption efficiency over time until it reaches a point where it does not offer any benefit over the base fluid alone, relevant to the solar absorption application.

4.5. Extinction coefficients

In Figure 4.5 the absorption behaviour of the carbon black nanofluid can be observed. Comparing the spectra of the solar simulator light to the transmission spectra of the carbon black nanofluid at different path lengths, it can be seen that there is a similar absorption behaviour across all the measured wavelengths. This shows that the carbon black nanofluid absorbs light across the entire UV-A, visible and near-infrared ranges. It is expected that the carbon black nanofluid will absorb

most of the UV-B radiation, as well as all of the wavelengths above 1000 nm which includes the near, mid and far infrared radiation ranges (Taylor et al., 2011a).

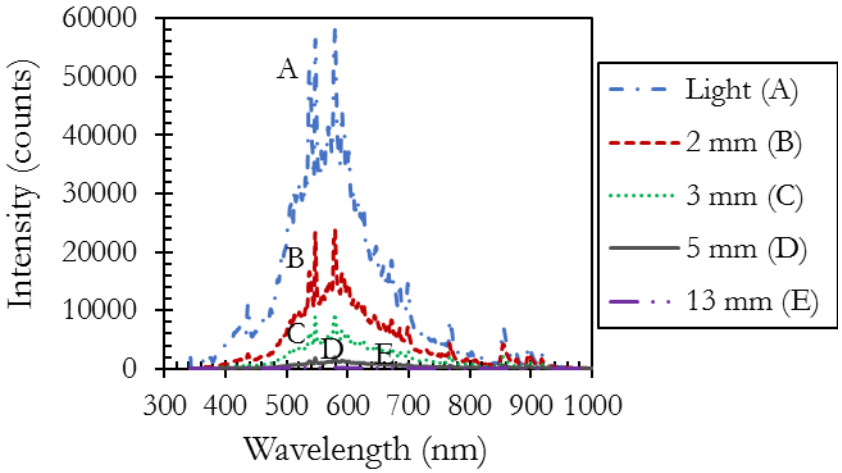

Figure 4.5: Absorption behaviour of carbon black nanofluid over light spectra at different path lengths.

The extinction coefficients across most of the visible light wavelengths (450 nm – 700 nm) were determined using an LED light. It is further deduced, from the results in Figure 4.5, that the trend that the extinction coefficients follow across the measured visible light region will be similar in the unmeasured UV range as well as the infrared range of the solar radiation spectrum.

To quantitatively compare the absorption properties of the different concentration carbon black nanofluids the Beer-Lambert law given in Equation 2 (Skoog et al., 2007, p. 336)), was used to determine the extinction coefficients of the nanofluids.

$$A = -\log\left(\frac{I}{I_0}\right) = \epsilon dc \qquad (2)$$

With A the absorbance,

I the light intensity transmitted through the sample (intensity counts),

I_0 the initial light intensity (intensity counts),

ε the extinction coefficient ($\frac{L}{cm \cdot g}$),

d the path length that light travels through the sample (cm),

c the concentration of the absorber ($\frac{g}{L}$).

To compare the extinction coefficients of the different carbon black concentration nanofluids, the concentration effects, present in the Beer-Lambert law, can be included in the extinction coefficient constant, thereby changing the extinction coefficient's units to 1/cm. The extinction coefficient then describes the amount of absorption of light that will be absorbed in one centimetre of a sample, regardless of the concentration of the nanofluid.

The Beer-Lambert law is, per definition, the linear relationship between concentration and absorbance. Therefore, the Beer-Lambert law can only be used to calculate the extinction coefficients if linearity can be proven between the concentration and absorbance. The Beer-Lambert law is limited to low analyte or particle concentrations because of this. At low concentrations there is sufficient distance between the particles in the solution that they do not influence each other's charge distribution, resulting in the linear relationship between concentration and absorption. At high concentrations the distance between the particles is reduced and particle-particle interactions occur to the extent that the particles' charge distribution is influenced by the adjacent particles. The additional forces between the particles and the related charge distribution changes, influence the absorption behaviour of the particles. These behavioural changes result in a

deviation from the linear relationship between concentration and absorption. The higher the concentration, the smaller the distance between particles are, the more the particles interact and the larger the deviations from linearity will be. (Skoog et al., 2007, p. 336-339).

In Figure 4.6 the absorption versus concentration relationship can be seen for different carbon black concentration nanofluids at the primary peak wavelength of the LED lamp (560 nm). For concentrations at and below 0.001 vol % carbon black, a linear relationship is present between the absorption and the concentration at a constant path length of 1 cm. At concentration above 0.001 vol % carbon black, a distinct non-linear trend is present.

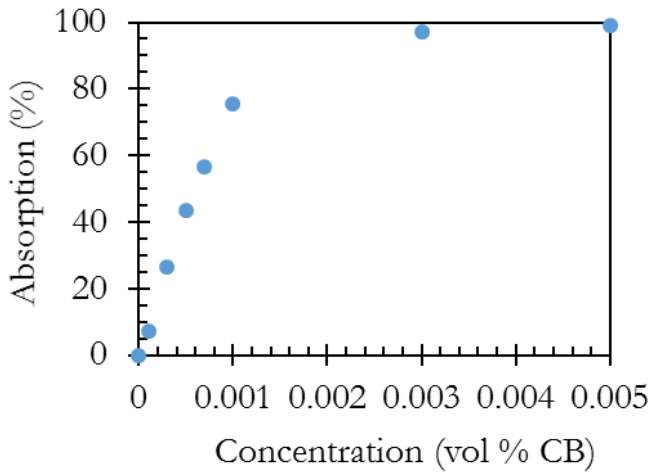

Figure 4.6: Absorption of different concentration carbon black (CB) nanofluids.

A linear trendline is fitted to the absorption data for carbon black concentrations at, and below 0.001 vol % in Figure 4.7.

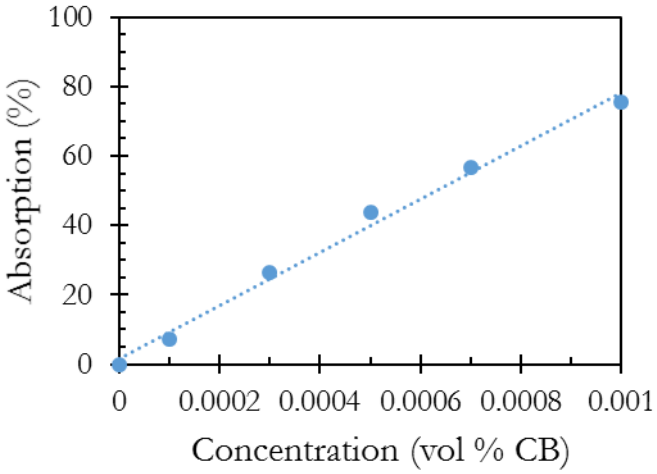

Figure 4.7: Relationship between concentration and absorption for low concentration carbon black (CB) nanofluids.

Since linearity between absorption and concentration is proven for concentrations at and below 0.001 vol %, the extinction coefficients can now be calculated using Equation 2 over the wavelength range of the LED light. The calculated extinction coefficients are shown in Figure 4.8.

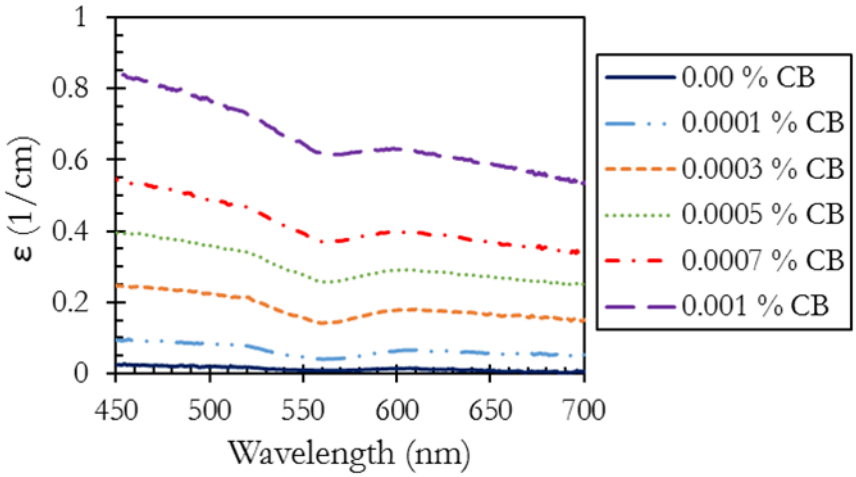

Figure 4.8: Extinction coefficient for different carbon black (CB) concentration nanofluids.

As can be seen from Figure 4.8 the carbon black nanofluids are consistently better at absorbing the lower wavelength light. The dip in the fairly negative linear trend,

is located at the primary peak wavelength transmitted from the LED lamp at 560 nm. It is furthermore pertinent to mention that the extinction coefficients for the 0.001 vol % carbon black sample is similar to that reported by Taylor et al. (2011a) for a 0.001 vol % graphite sample.

From the extinction coefficients in Figure 4.8 it is seen that the carbon black nanofluids are better at absorbing lower wavelength radiation. This trend is consistent with most types of water based nanofluids. What is also consistently shown, for all water based nanofluids reported in other studies, is an increase in the extinction coefficients at and above 900 nm wavelengths. This is due to the fact that water is an excellent absorber of the infrared wavelength region and dominates the absorption in this region (Saroha et al., 2015). Therefore, the carbon black nanofluid shows good absorption properties over the whole solar spectrum with the carbon black particles dominating the absorption in the UV and visible light regions (280 nm – 900 nm) and the base fluid of salt water dominating the absorption throughout the infrared regions (> 900 nm).

Looking at the performance comparison of the different carbon black concentration nanofluids' absorption, it can be seen that even the extremely low carbon black concentration nanofluids have a distinct absorption improvement over that of salt water in the visible range tested. The absorption improvement at the wavelength of 560 nm of the different carbon black concentration nanofluids is shown in Figure 4.9.

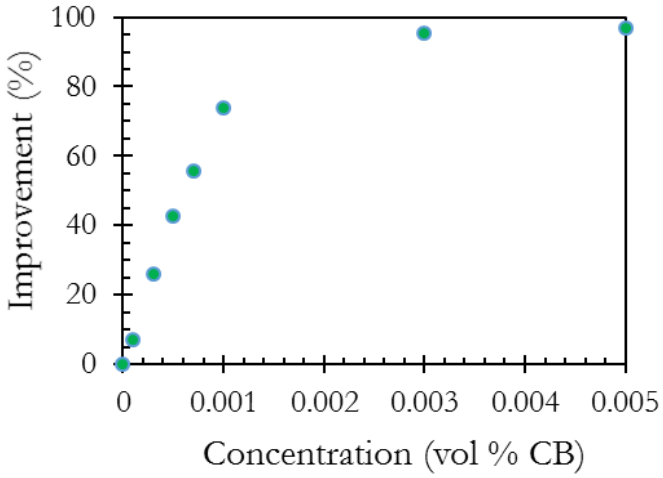

Figure 4.9: Absorption property improvement of different carbon black (CB) concentration nanofluids compared to that of the base fluid.

4.6. Nanofluid stability

For the purpose of the application, a specific nanofluid will only be used once. Therefore, the timespan the nanofluid needs to be stable is not extensive and only needs to be stable under storage conditions. It does not need to withstand several heating cycles. The stability time will however, impact the nanofluid production batch size and the time of production when taking into account the final application.

Photographs were taken on consecutive days over a time span of 31 days for carbon black nanofluids with different concentrations. The relevant photos are shown in Figure 4.10.

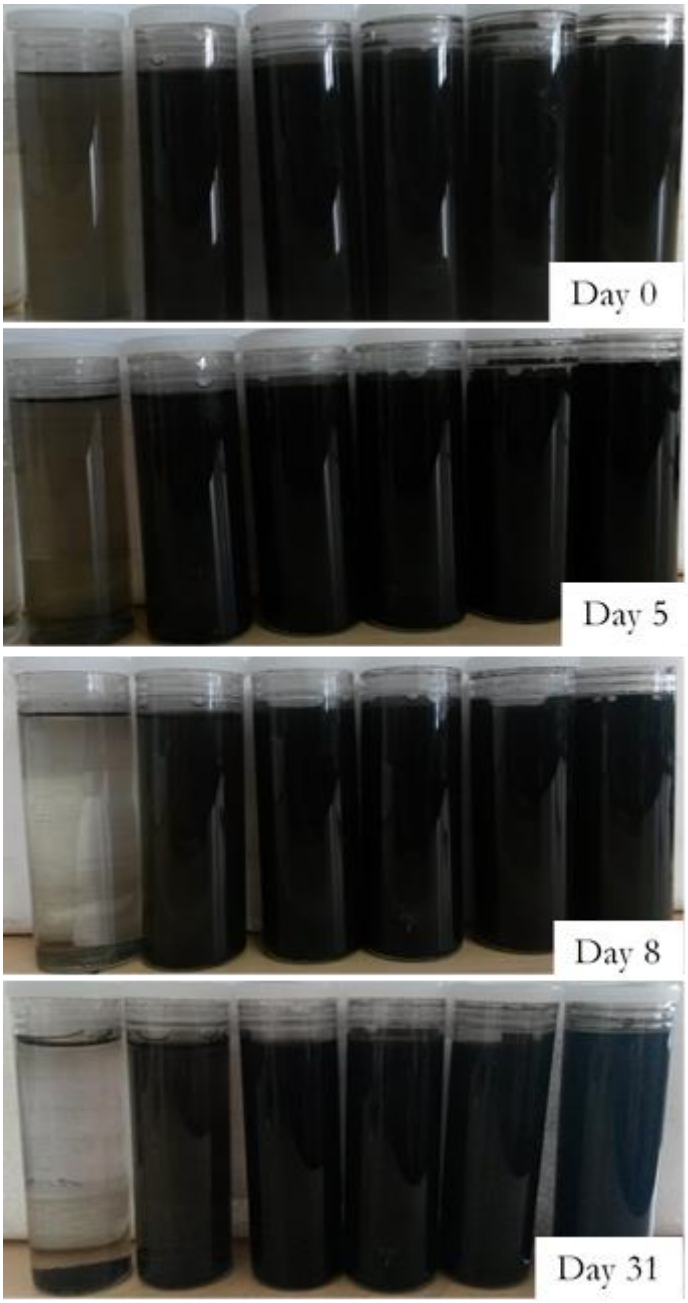

Figure 4.10: Visual behaviour of carbon black nanofluids over time. Concentrations used from the left: 0.0005 vol %, 0.001 vol %, 0.003 vol %, 0.005 vol %, 0.01 vol % and 0.05 vol %.

From Figure 4.10 it can be seen that there is no visible change in the appearance of the different concentration nanofluids until day 8. On day 8 it can be seen that the carbon black particles in the 0.0005 vol % carbon black nanofluid have settled out of the bulk solution. No further changes can be seen in the other concentration

nanofluids for the remaining time. This shows that the nanofluid has a visual stability of at least 31 days. The lower concentration nanofluids in the range (0.001 vol %, 0.003 vol %) started settling out after 38 days and the 0.005 vol % nanofluid at 50 days. The 0.01 vol % and 0.05 vol % carbon black nanofluids remained stable for multiple months. Figure 4.11 shows 0.05 vol % carbon black nanofluids that have been produced at different times and Figure 4.12 shows the particle size analysis for two of the 'aged' nanofluids.

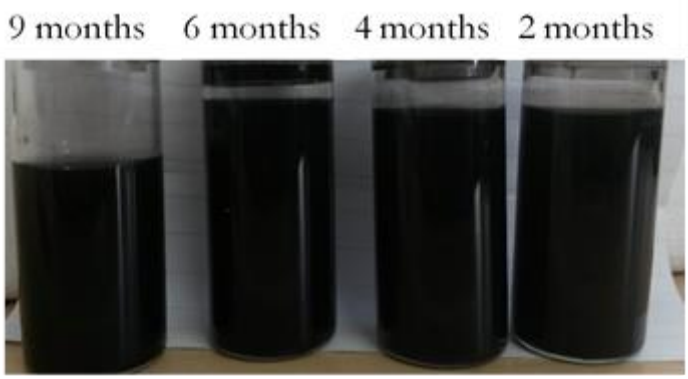

Figure 4.11: 0.05 vol % carbon black nanofluids over several months.

From Figure 4.11 it can be seen that even after 9 months there is no visible settling of the nanofluid.

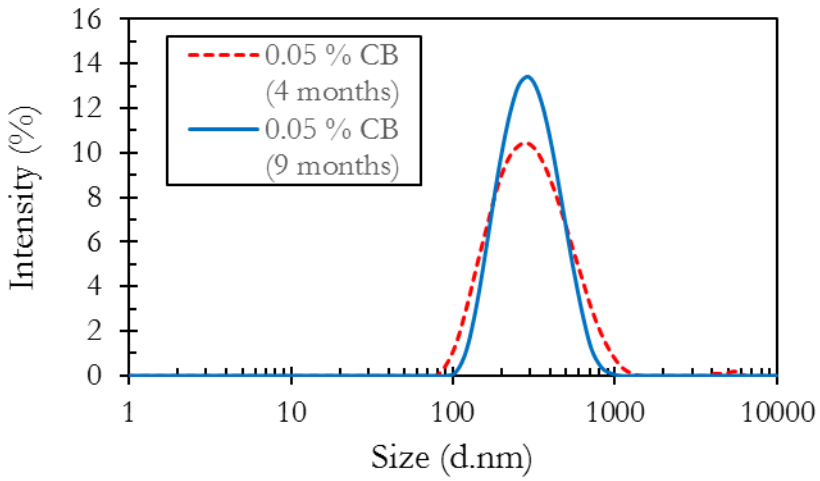

Figure 4.12: Particle size distribution for aged carbon black (CB) nanofluids.

From the particle size distribution, shown in Figure 4.12, it can be seen that the suspended particles have sizes between approximately 90 nm and just above 1000 nm, with an average hydrodynamic diameter of 263 nm for the 4-month-old sample and 270 nm for the 9-month-old sample. There are only slight differences from the particle size distributions seen in the freshly prepared samples in Figure 4.2 in the previous section and these differences are more likely due to slight differences in the samples than from additional agglomeration.

In all of the samples the same trend is visible: that the lower concentration carbon black nanofluids visibly settles out first. The reason for the effect the carbon black concentration has on stability is uncertain. It is possible that the increased number of particles results in smaller distances between particles, thereby stabilising the particles electrostatically (Fendler, 2001). It is also possible that it is due to the two-step production method. When the nanoparticles are treated with the surfactant prior to suspension in the base fluid, there is inevitably a fraction of carbon black nanoparticles that does not get wetted. This unwetted fraction of particles is dispersed homogeneously in the base fluid after sonication. However, as the nanofluids are synthesised from the masterbatch solution, these unstable particles are inevitably also added to the sample and will settle out faster than the wetted nanoparticles. This fraction unwetted nanoparticles settles out of the bulk fluid first and, because there are less particles in the lower concentration nanofluids, the settling is visually observed in them first. It has to be stressed at this point that the two theories mentioned above are just possible explanations. The reason for the effect of the carbon black concentration on the stability can also be a combination of the two proposed phenomena or be dependent on other factors all together. To ascertain the reason for the nanoparticle concentration-stability relationship, additional experimental work is required.

Further tests were done to find a more quantitative method to infer the stability of the colloidal suspension. Absorption tests, similar to the tests done to determine the extinction coefficients, were done and repeated after three days. The results are shown in Figure 4.13.

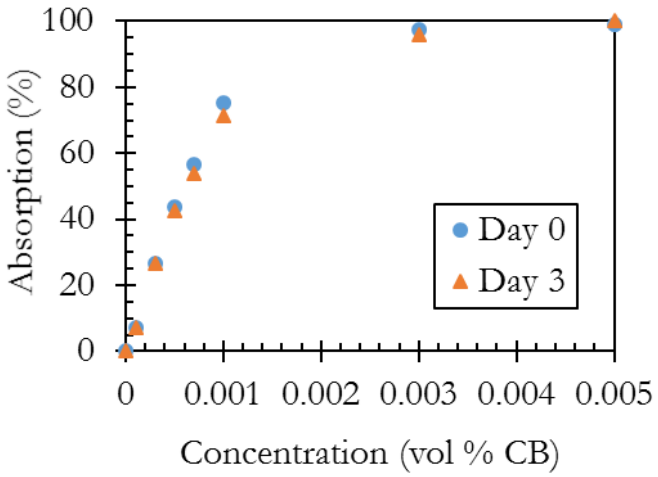

Figure 4.13: Absorption properties of carbon black (CB) nanofluids comparison after 3 days.

From Figure 4.13 it can be seen that there is no significant difference in the optical properties of the carbon black nanofluids except for the 0.001 vol % sample. It is expected that the difference at that concentration is because of variance in the optical setup. It is however, still a small difference of only 3 %. This shows that, as expected, there is no significant change in the nanofluid's effective concentration after 3 days.

From all of the above results it is concluded that the nanofluids used can be classified as stable for the application they are intended for, which includes being heated only once for the purposes of a flash type desalination process.

4.7. Photothermal properties

The photothermal properties of the carbon black nanofluids were measured on multiple days and similar trends were seen on all days. The data in Figure 4.14 was taken on a cloudless summer day at the University of Pretoria with an average DNI of 950 W/m^2 for the duration of the experiments. The solar radiation data used was taken as minute averaged for the experiment time from the SAURAN database, taken at the UPR - GIZ University of Pretoria station (Brooks et al., 2015).

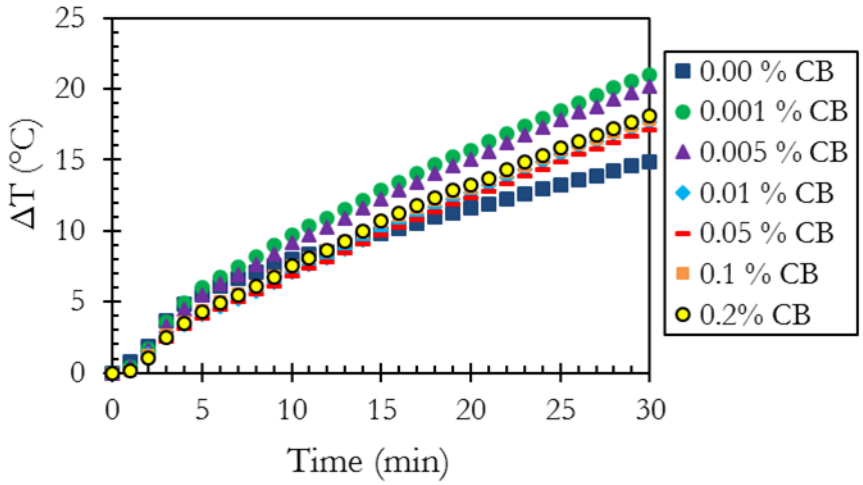

Figure 4.14: Photothermal properties of different carbon black (CB) concentration nanofluids.

From Figure 4.14 it can be seen that the lower concentration carbon black nanofluids showed slightly better photothermal properties, but not to a significant extent. It is believed that the difference in the heating rates of the nanofluids is caused by the position of absorption in the nanofluid, rather than the amount of solar irradiation being absorbed. From the absorption properties shown in Figure 4.3 it is known that at lower concentrations the solar irradiation will penetrate deeper into the fluid, heating the bulk fluid, whereas at the higher concentrations all of the irradiation is absorbed at the surface of the polytop tube. This will result

in higher temperatures at the surface of the tube and therefore more convective losses to the environment, as supported by the findings in Taylor et al. (2011b). These results, however, differ from a similar study conducted by Han et al. (2011). They found that with an increase in carbon black concentration, there is an increase in the photothermal properties. The study was conducted at very high concentrations (3.3 % carbon black and higher).

4.8. Concentrated solar irradiation penetration depth into stagnant nanofluid

The absorption depth data for each concentration can be seen in Figure 4.15 to Figure 4.20. Where relevant a photo of the light that passed through the container is added as a secondary figure.

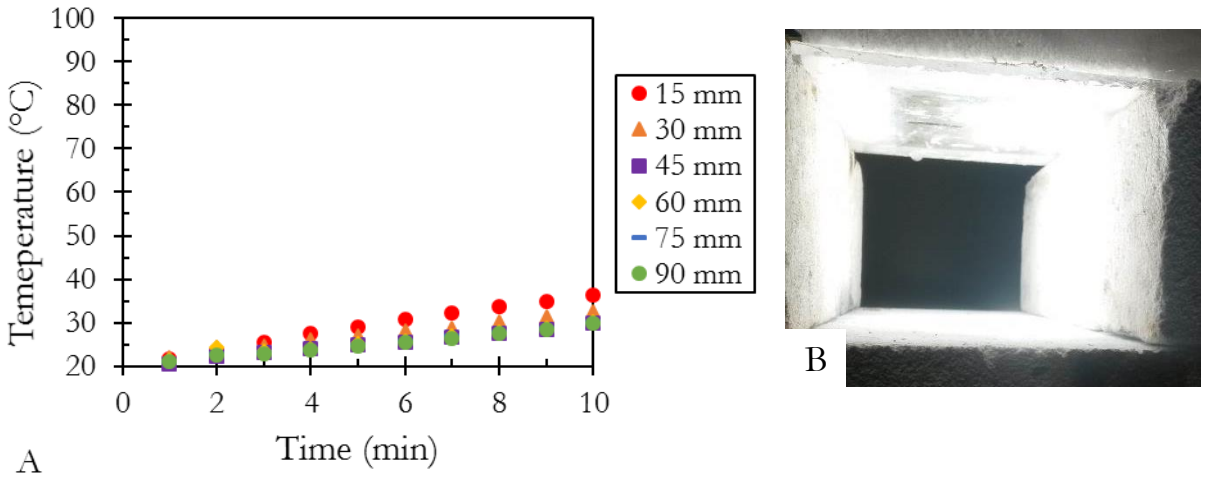

Figure 4.15: A: Temperature increase profile for salt water at different depths. B: Photo at bottom of container.

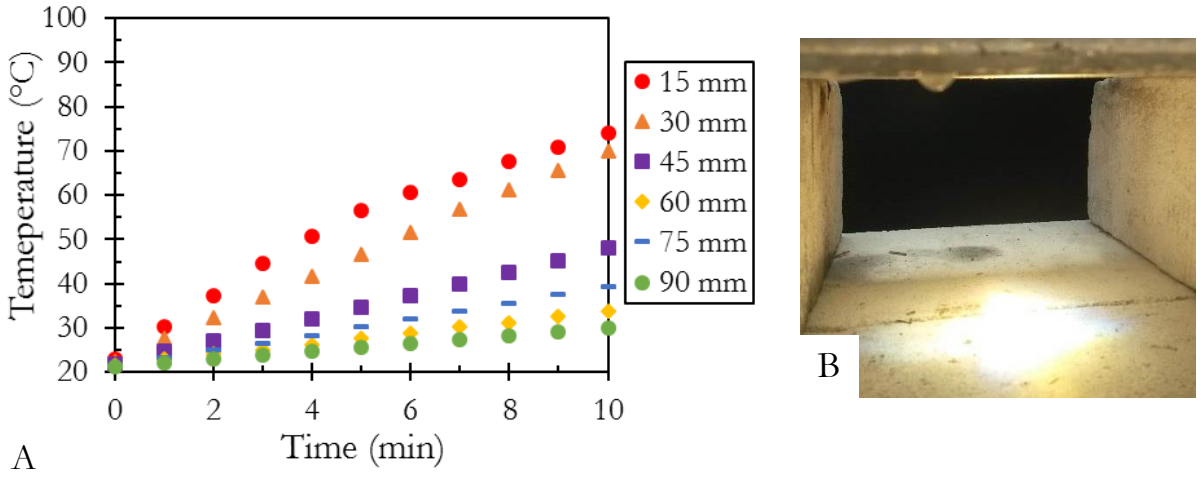

Figure 4.16: A: Temperature increase profile for 0.0005 vol % carbon black nanofluid at different depths. B: Photo at bottom of container.

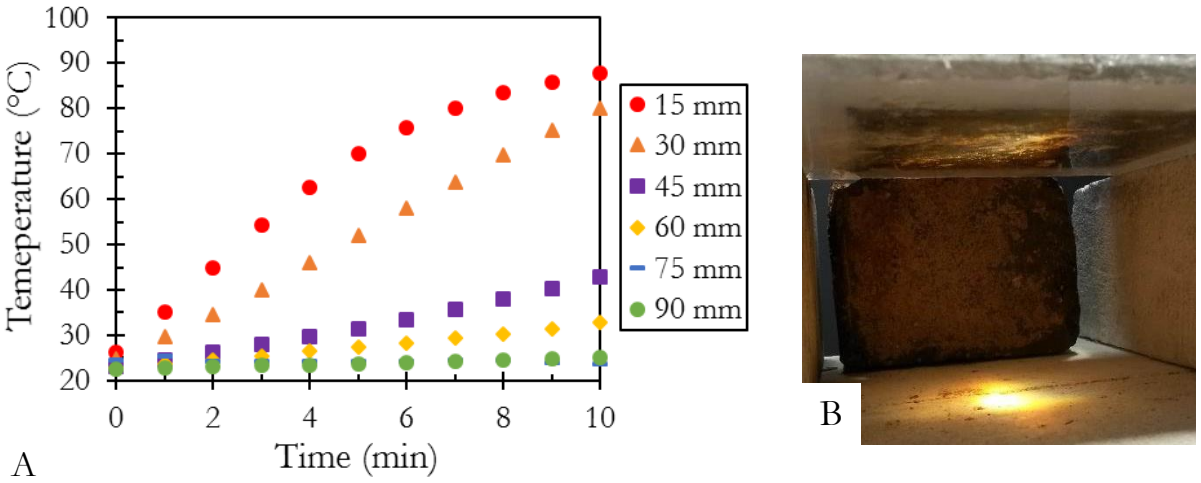

Figure 4.17: A: Temperature increase profile for 0.001 vol % carbon black nanofluid at different depths. B: Photo at bottom of container.

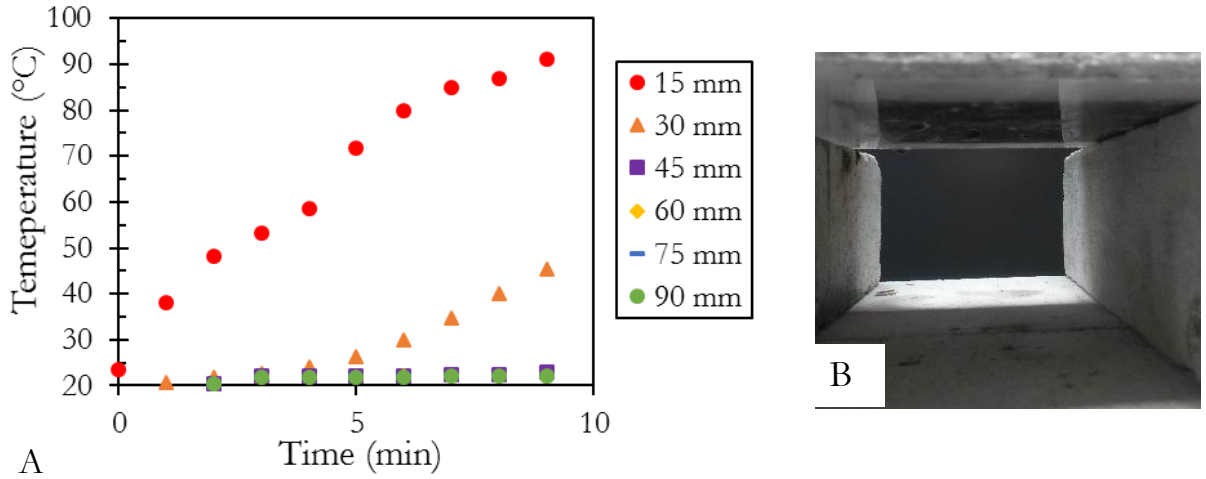

Figure 4.18: A: Temperature increase profile for 0.005 vol % carbon black nanofluid at different depths. B: Photo at bottom of container.

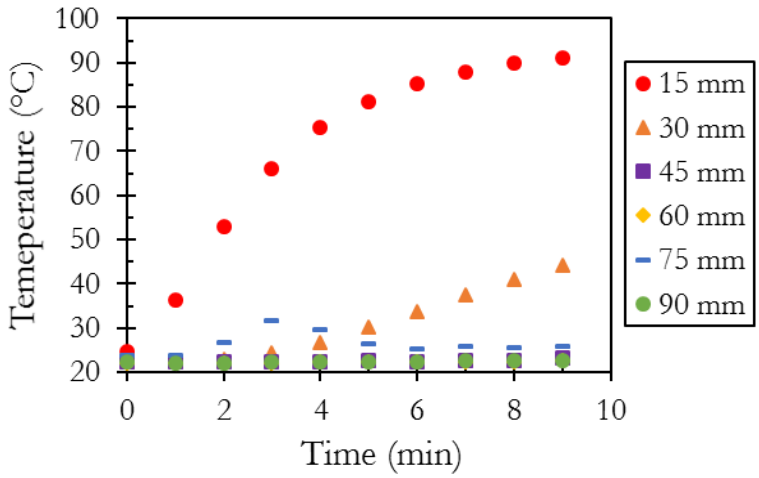

Figure 4.19: Temperature increase profile for 0.01 vol % carbon black nanofluid at different depths.

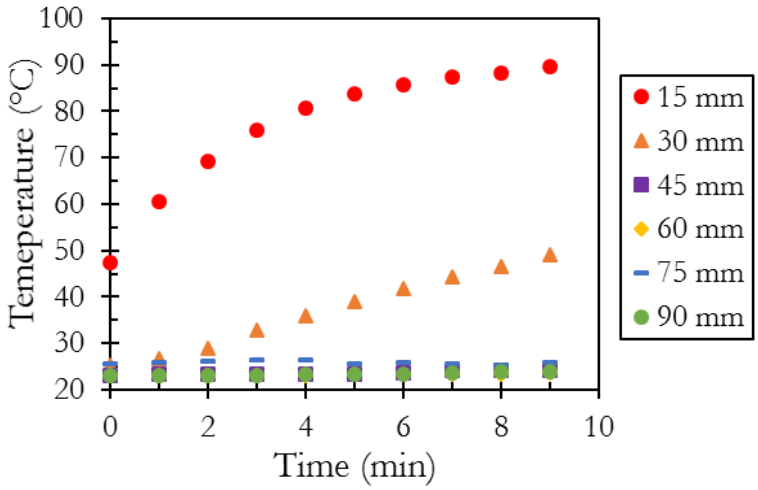

Figure 4.20: Temperature increase profile for 0.05 vol % carbon black nanofluid at different depths.

From Figure 4.15 it can be seen that the salt water does not absorb much of the solar irradiation, as determined from Figure 4.15 A, because of the lack of temperature increase and in Figure 4.15 B, from the intense light that exits the container at the bottom. It should also be noted that the thermocouples at all depths, temperature is increasing in a similar way.

From Figure 4.16 A, it can be seen that even at such low concentration as 0.0005 vol % carbon black the degree of energy absorption increases significantly where a maximum temperature of 75 °C is reached in 10 min. From Figure *4.16* B, it can still be seen that there is a lot of irradiation exiting at the bottom of the container. Using the MP-200 pyranometer the exiting irradiation was attempted to be measured but it exceeded the maximum reading of 1500 W/m^2. All of the depths show an increase in temperature, although different to the salt water the top liquid is heated faster than the bottom liquid, as is expected, because the irradiation that reaches the bottom has a lower intensity. The top two thermocouples show similar temperature values after 10 minutes.

From Figure 4.17 A, it can be seen that 90 °C was approached after 10 minutes at depths of 15 mm as well as 30 mm for a carbon black nanofluid with a

concentration of 0.001 vol %. From Figure 4.17 B, it can be seen that there still exits light from the bottom of the container. Using the pyranometer an energy value of 1100 W/m^2 was measured. It is also seen that although light passes through, there is not significant heating below 60 mm.

From Figure 4.18 it can be seen that, for a nanofluid of 0.005 vol % carbon black, there is a much higher temperature gap between the 15 mm and 30 mm thermocouple, where the temperature at 30 mm depth only starts rising at 5 minutes. It is believed that this temperature increase is more due to conduction from the top layer than from irradiation absorption. It should be noted that for this configuration very little convection in the fluid is expected, due to the thermal stratification: i.e. the lower density, higher temperature water layers should be stable above the higher density colder layers. From Figure 4.18 B, it can be seen that no light passes through the nanofluid at this concentration or higher concentrations. There is no heating for the liquid below 30 mm that shows that all the significant energy is absorbed in the top 30 mm layer.

From Figure 4.19 it can be seen that the top layer of the 0.01 vol % carbon black nanofluid heats up faster than at lower carbon black concentrations. The second layer, at 30 mm, also starts heating at an earlier time (4 minutes). This could be an indication of a higher thermal conductivity because of the higher concentration of carbon black. There is no other significant heating in the layers below 30 mm. It should be noted that the temperature profile of the thermocouple at 75 mm is an anomaly and attributed to experimental error because there is no heating at 60 mm or 90 mm.

The 0.05 vol % carbon black nanofluid in Figure 4.20 shows similar results to the 0.01 vol % carbon black nanofluid in Figure 4.19, except that the 30 mm layer starts heating earlier, at 2 minutes for the 0.05 vol % carbon black, compared to the 4 minutes for the 0.01 vol % carbon black. This supports the theory that all the significant energy is absorbed in the top 15 mm layer and the second layer at

30 mm is heated by conduction and that at higher concentrations carbon black the nanofluid has a higher thermal conductivity that leads to faster heating of the second layer.

There was a very rapid transition between 0.001 vol % carbon black and 0.005 vol % carbon black nanofluids in the penetration depth of the solar irradiation. Where there is still unused light passing through at 0.001 vol % and at 0.005 vol % there is no distinct heating in the 30 mm layer. It is difficult to draw conclusions regarding the overall absorption efficiency of the system from this data since a critical energy flow is unaccounted for, namely, the amount of evaporated/boiled water. Presumably, once the carbon black concentration is high enough to heat the upper fluid layers to temperatures approaching the normal boiling point, these losses are significant.

4.9. Pilot scale concentrating rig characterisation

The optical energy losses in the concentrating steps, measured using a pyranometer, after every individual optical step immediately after the cleaning of all optical surfaces, are shown in Table 4.1. The data was measured on four different days and showed a less than 2 % difference on the different days. The average value is reported in Table 4.1.

Table 4.1: Optical energy losses per concentration step for clean optical surfaces.

Concentrating stage	Losses (%)
Mirror 1	27
Mirror 2	30
Fresnel lens	9
Total losses	53

The optical energy losses for the system are detrimentally high, with the majority of the losses occurring from the mirrors. The energy losses for an uncleaned system reached as high as 70 %, depending on the amount of dust on the optical surfaces.

4.10. Flow cell experiments

4.10.1. Solar collector size

The first collector that was designed, built and implemented was a 2.5 cm deep collector with a 5 cm x 5 cm collection area. This collector was designed to operate at the focal point at a concentration ratio of 1100. At this concentration ratio however, the carbon black nanofluid in the smaller volume collector, almost immediately upon exposure to the concentrated irradiation, vaporised and the temperature of the steam destroyed the collector. From this result it was decided to increase the size of the solar collector's collection area to 10 cm x 10 cm and reduce the concentration ratio to 100. This decreased the thermal stress on the collector's building materials to manageable levels and made it possible to keep using the inexpensive building materials that also improves the manufacturability of the solar collectors.

4.10.2. Heating rate experiments

The flow cell experiments are the first step towards the ultimate application of CSP driven desalination. In Figure 4.21 the normalised temperature increase data can be seen for a flow rate through the solar collector of 50 mL/min. This is a very low flow rate and serves to compare the heating rates of the nanofluids in the collector. At this low flow rate the fluid's temperature in the collector kept rising, despite some flow being present. The terminating factor for the experiment was when vapour formation was present in the collector. The temperature at which

bubble formation was first visible was approximately 90 °C. The data was normalised to make the data of the different experimental runs comparable. This normalisation was achieved by dividing the change in temperature with the average DNI measurement value (from the SAURAN database (Brooks et al., 2015)) for the timespan of the experimental run. This is the radiation energy reaching the primary mirror and not the energy that reaches the nanofluid, but it shows the change in energy available to the fluid during the experiment and therefore serves as a good normalisation value. The experiments were performed in a 2.5 cm deep collector with a single-pane, 3 mm thick polycarbonate lid. The experiment was repeated three times and the outlet temperature values were within 5 % of each other.

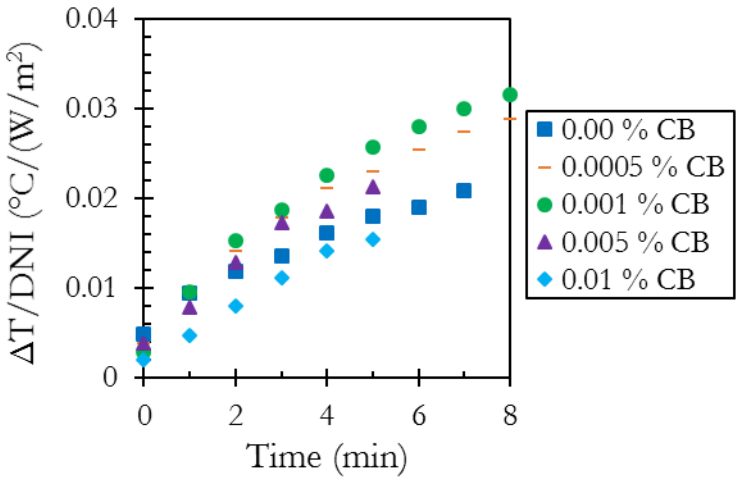

Figure 4.21: Temperature increase for 50 mL/min flow rate of different carbon black (CB) concentration nanofluids.

For the higher carbon black concentrations of 0.005 vol % and 0.01 vol % bubbles formed much faster than for the nanofluids with lower carbon black concentrations. For the 0.01 vol % carbon black nanofluid the vapour was forming at an outlet temperature as low as 38 °C. This supports the findings from the photothermal properties experiments in Figure 4.14, that for high concentrations of carbon black all of the solar irradiation is absorbed close to the

surface of the collector and localised boiling occurs without the bulk fluid being heated. This will lead to increased convective losses from the surface of the collector. To compare the heating rates and estimate the increase in concentrated solar irradiation absorption efficiency of the different concentration nanofluids, the normalised temperature difference after 5 minutes of operation time, of the different carbon black concentration nanofluids, were compared to that of the salt water reference run. The comparison can be seen in Table 4.2.

Table 4.2: Comparison of heating rates for different carbon black concentration nanofluids at 50 mL/min compared to that of the base fluid.

Carbon black concentration (vol %)	Heating rate improvement (%)
0.00	0
0.0005	27
0.001	42
0.005	18
0.01	-14

From Table 4.2 it can be seen that 0.001 vol % carbon black nanofluid performed the best with a 42 % faster heating rate than that of salt water for the case of a 2.5 cm deep collector. This is due to the fact that all of the solar irradiation is absorbed, but the concentrated solar irradiation penetrates deep enough into the fluid allowing the bulk fluid to be heated. At concentrations below 0.001 vol % carbon black, not all of the irradiation is absorbed and higher reflective losses result in lower efficiencies. At higher concentrations, the majority of the irradiation is absorbed close to the surface resulting in the bulk fluid not being heated as efficiently and increased convective losses present due to a higher temperature at the lid of the collector. A surprising occurrence was found for the 0.01 vol % carbon black nanofluid, that showed a worse performance than the salt

water alone. This is not because there is reduced solar absorption, but due to the significant increase in the temperature at the lid of the collector that is leading to increased convective losses from the collector. It should be kept in mind that the data from Table 4.2 is for the specific case of a 2.5 cm deep collector at a concentration ratio of 100. This data shows that to use the optimal carbon black concentration for a specific application is critical towards the efficiency of the system. If the incorrect concentration is used, it can (as in the case of the 0.01 vol % carbon black nanofluid) lead to the system being less efficient than when the base fluid is used alone.

4.10.3. Stagnant vs flowing nanofluid behaviour

In the last few years there has been an extensive amount of research done on nanofluids and a large number of the studies on the solar energy applications of nanofluids. Very little research has of yet been dedicated to nanofluids implemented in concentrated solar power applications. The studies that looked at high intensity irradiation of nanofluids focused on the behaviour of stagnant nanofluids where the only movement of the nanoparticles is a result of Brownian motion and buoyancy driven flow. The behaviour of stagnant nanofluids exposed to a high intensity localised light source (e.g. laser beam or concentrated solar irradiation) has been studied, among others, by Taylor et al. (2012) and Neumann et al. (2013). They found that there is superheating of the nanoparticles occurring at the surface of the nanofluid-light interface. This results in immediate nucleate boiling and bubble formation on the surface of the nanoparticles, which relates to vapour generation while the bulk fluid still remains far below the boiling point. This behaviour was witnessed in the concentrated solar irradiation penetration depth into stagnant nanofluid experiments conducted in the previous section where, immediately on exposure to the concentrated solar irradiation, steam could be seen rising from the surface of the nanofluid. This phenomenon was however,

absent for all cases in the flow cell experiments. For the heating rate experiments at low flow rates (50 mL/min) and high carbon black concentrations (above 0.005 vol %) there were very fast, but not immediate, bubble formation against the lid of the flow cell without the bulk fluid being heated. The concentrations below 0.005 vol % only started to form bubbles after several minutes at a flow rate of 50 mL/min and never formed bubbles at higher flow rates.

From these observations, a hypothesis is suggested that there exists an absorption dependence on the linear velocity of the particles in the fluid. When there is an additional external driving force moving the nanoparticles, it relates to an increased amount of nanoparticle interactions. These increased interactions between the particles, also increases the extinction coefficient and thereby the absorption behaviour of the nanofluid with the same reasons as why the Beer-Lambert law is a limiting law and only applicable to low concentration solutes that do not show particle-particle interactions (Skoog et al., 2007, p. 336-339). This increased amount of interactions also allows the superheated individual particles to interact with other particles and conduct their heat to neighbouring particles, thereby heating the bulk fluid. The flowing nanofluid therefore, not only shows increased absorption properties because of an increased extinction coefficient at the same carbon black concentration, but also harnesses the concentrated solar energy to heat the bulk fluid in contrast to the stagnant nanofluid harnessing the energy for vapour generation.

4.10.4. System efficiency

The efficiency was calculated using Equation 3.

$$\eta = \frac{\dot{m}C_P\Delta T}{DNI} \tag{3}$$

With η the efficiency (%),

$\dot{m}$ the mass flow rate ($\frac{kg}{s}$),

C_P the heat capacity of the nanofluid ($\frac{J}{kg \cdot K}$),

ΔT the temperature difference over the collector (K),

DNI the direct normal solar radiation available to be used ($\frac{W}{m^2}$).

Equation 3 was used to calculate the collector, as well as the overall system efficiency. The only difference being the amount of energy that is available to the collector (DNI value). The overall system efficiency is calculated using the DNI before the irradiation has gone through any of the optical concentrating steps, therefore the amount of solar irradiation that would be available in a non-concentrating system with a collector with a 1 m^2 collection area. The collector efficiency uses the DNI that is available to the collector, therefore the solar radiation available after all of the optical concentrating steps. This is the solar radiation measured after the Fresnel lens. 1 m^2 of solar radiation is, consistently throughout the experiments, concentrated on the 10 cm x 10 cm collector's collection area. Therefore, the DNI used is in units of W/m^2 and not converted to $W/(10\ cm^2)$, as this would yield the same results. The collection area of 10 cm x 10 cm relates to a concentration ratio of 100. This means that the energy heat flux experienced on the collector's surface is 100 times that of the heat flux experienced on the Fresnel lens's optical step. This varies of course with the DNI

solar irradiation levels per experiment, but was approximately 500 W/m^2 after the Fresnel lens. Therefore, the heat flux experienced on the 0.1 m^2 collection area was 50 000 W/m^2.

It is unfortunate that the fluid efficiency could not accurately be determined due to the lack of information regarding the losses from the collector. Through the optical steps the solar radiation is first reflected from the primary mirror, on the solar-tracking system, onto the secondary mirror that reflects the light down through the Fresnel lens. The Fresnel lens refracts the light onto a point. This refracted light hits the collector at different angles depending on where on the Fresnel lens it is refracted from, as shown in Figure 3.7. The increased incident angle will relate to an increase in reflective losses from the collector's surface. However, because of the intensity of the light and the operating limitation of the optical characterisation equipment these increased reflection losses could not be measured. Another source of losses that was not accounted for, was the extent to which the collector building material was heated. The extruded polystyrene foam was chosen partly because of its insulating ability, but there will still be some extent of heating of the foam. Due to all of the uncertainties, no informed assumption could be made about the losses from the collector to estimate a reliable fluid efficiency from these experiments.

In the following sections, different parameters, both the design aspects as well as operational aspects, and their effect on the collector efficiency, were investigated. It is very important, however, to keep in mind that because of the various influencing variables, only the variables changed in an experiment, can be compared. Because of the complexity of the nanofluid's behaviour, no single experiment allowed distinct behaviours to be observed. Trends however, were visible when looking at specific variables.

4.10.4.1. Collector's lid design effect on collector efficiency

It is important to analyse the effect of the collector design parameters on the collector's efficiency to be able to better interpret the effect of the operational variables on the collector's efficiency. In Figure 4.22 the comparison of a single-pane lid vs a double-pane lid, where there is a 3 mm spacing between the panes, is compared in terms of the efficiency achieved for a 2.5 cm deep collector at a flow rate of 250 mL/min.

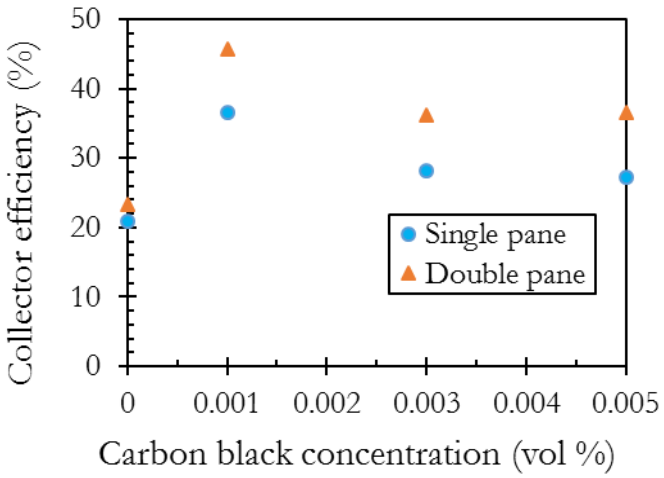

Figure 4.22: Collector's lid design effect on collector efficiency.

From Figure 4.22 it can be seen that the double-pane allows a higher efficiency to be achieved for all carbon black concentration nanofluids. This is despite the fact that there is inevitably an increase in reflective, as well as transmittance losses through the double-pane lid, compared to that of the single-pane lid. This means the reduction in convective losses is higher than the increase in optical losses. The double-pane lid reduces the heat losses from the system because the heat transfer resistance network is extended with the addition of the air gap between the panes as well as the extra pane. The temperature difference necessary for heat transfer is also reduced with the heated air in the gap between the panes. The heat transfer coefficient for air is also much less than the conductive heat transfer coefficient of polycarbonate, resulting in a reduction of convective losses.

4.10.4.2. Collector depth's effect on collector efficiency

Two collector depths were investigated in order to determine the effect of the absorbing path way length on the collector's efficiency. The experiments were done in collectors with double-pane lids and the different collector depths as indicated with a nanofluid flow rate of 250 mL/min. The results can be seen in Figure 4.23 for the three lower carbon black concentration nanofluids. Only the lower carbon black concentration nanofluids were tested because an increase in absorption path length will not benefit the higher concentration nanofluids, as all of the concentrated irradiation is already absorbed in a 2.5 cm deep collector, as seen from the heating rates experiment.

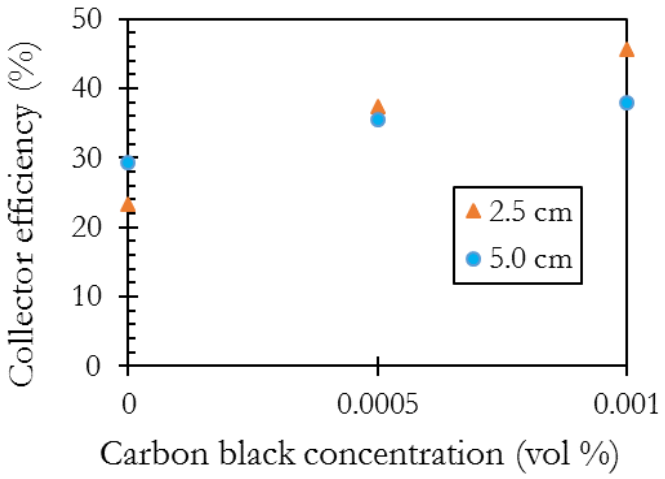

Figure 4.23: Collector depth's effect on collector efficiency.

From Figure 4.23 it can be seen that, as expected, the efficiency of the salt water without carbon black has a higher efficiency with a longer absorbing path length. It is interesting though, that the there is no increase in efficiency for the 0.0005 vol % carbon black nanofluid in the deeper collector. This can either be a manifestation of the error margin in the experimental setup, or it can possibly also point to an absorption-flow rate dependence. If the idea of an absorption-flow rate dependence is entertained, the result can be explained as follows: although there is a longer path length available for absorption, the linear velocity for the same flow

rate is reduced because of a larger volume collector. This reduction in the linear velocity that the nanoparticles are moving at, reduces the particle-particle interactions, reducing the extinction coefficient (compared to that of the 2.5 cm deep collector) and thereby reducing the absorption properties of the nanofluid. The similar performance for the two collector depths therefore reflects a point at which the velocity effects and the concentration effects is at equilibrium. For the 0.001 vol % carbon black nanofluid it can be seen that the deeper collector is less efficient than the shallower collector. This is due to the fact that complete absorption already occurs at 2.5 cm and the additional absorbing path length leads to the bulk fluid not being heated.

4.10.4.3. Carbon black concentration's effect on collector efficiency

As found and mentioned in the previous experiments done concerning the absorption properties, photothermal properties and extinction coefficients of the nanofluid, the carbon black concentration of the nanofluid is the most important variable to influence the collector design and thereby the efficiency of the system. If the concentration is too low, not all of the solar irradiation will be absorbed resulting in inefficiencies. If the concentration is too high, all of the solar irradiation is absorbed in a thin layer close to the lid, resulting in an unheated bulk fluid and higher convective energy losses from the top of the system, which may even result in a less efficient system than when not using a nanofluid, as was seen from the heating rate experiment in the previous section. In Figure 4.24 the effect of the carbon black concentration in the nanofluid on the collector efficiency can be seen. This data is for a 2.5 cm deep collector with a double-pane lid, varying the carbon black concentration in the nanofluid at a flow rate of 250 mL/min.

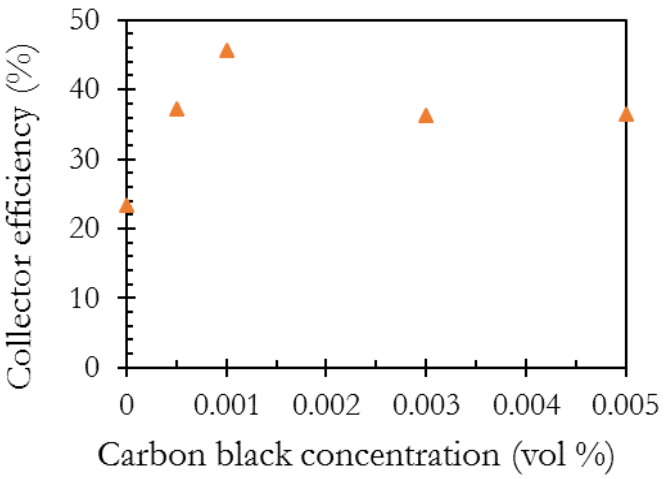

Figure 4.24: Carbon black concentration's effect on collector efficiency.

As expected from the previous experiments, there is an optimum carbon black concentration in the middle of the range of concentrations tested. At 0.001 vol % the system shows a maximum efficiency, which coincides with the results from the photothermal property tests as well as the heating rate experiments. It can also be seen from Figure 4.24 that the collector efficiency for that of the higher concentrations of 0.003 vol % and 0.005 vol % is very similar to that of the lower 0.0005 vol % carbon black nanofluid. This suggests that there is a trade-off between the losses from the system using a low carbon black concentration nanofluid (where not all of the solar irradiation is absorbed), and the higher convective losses from the system using higher carbon black concentration.

4.10.4.4. Flow rate's effect on collector efficiency

The effect of flow rate on the collector efficiency is expected to be primarily caused by the decrease in convective losses from the system related to the lower residence time of the nanofluid in the collector at higher flow rates, leading to lower outlet temperatures. The outlet temperature from the collector as the flow rate increases can be seen in Figure 4.25. It should be kept in mind that the outlet temperature is not necessarily an indication of the efficiency of the system as the solar irradiation value is not taken into account.

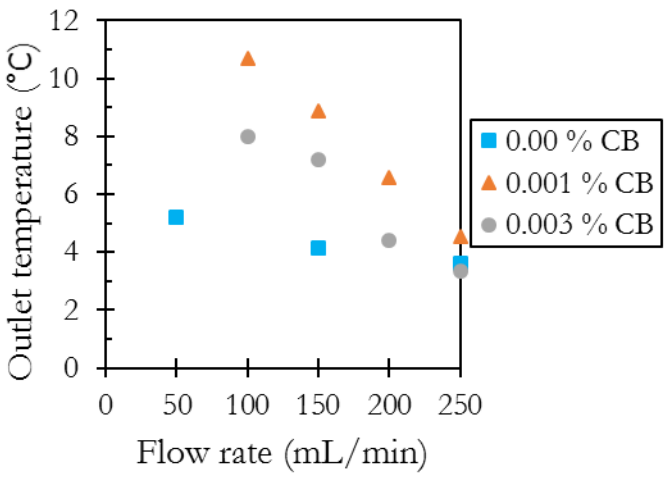

Figure 4.25: Flow rate's effect on the outlet temperature of the nanofluid from the collector.

As the flow rate increases, the time that the nanofluid is exposed to the solar irradiation is reduced and the outlet temperature decreases. Due to this reduction in the outlet temperature, the convective losses from the lid of the collector are reduced, because the temperature difference (energy loss driving force) between the lid and the ambient air is reduced. From Figure 4.25 it can also be seen that the temperature reduction due to flow rate is not as significant for the salt water as for the nanofluids.

In Figure 4.26 the effect that the nanofluid flow rate has on the collector efficiency can be seen for different carbon black concentration nanofluids. This data is for a 2.5 cm deep collector with a single-pane lid. It is pertinent to mention that the results of the varying flow rate experiments can't be compared to that of the varying carbon black concentration experiments because of the differences in the design of the collectors. The data is reviewed and compared for experiments that are comparable to each other (e.g. done with the same collector on the same day). This is because of the complexity and lack of full understanding of the nanofluid-concentrated sunlight system that can easily lead to conclusions being drawn that is

not based on the behaviour of the nanofluid under concentrated irradiation, but the inherent difference between the collectors.

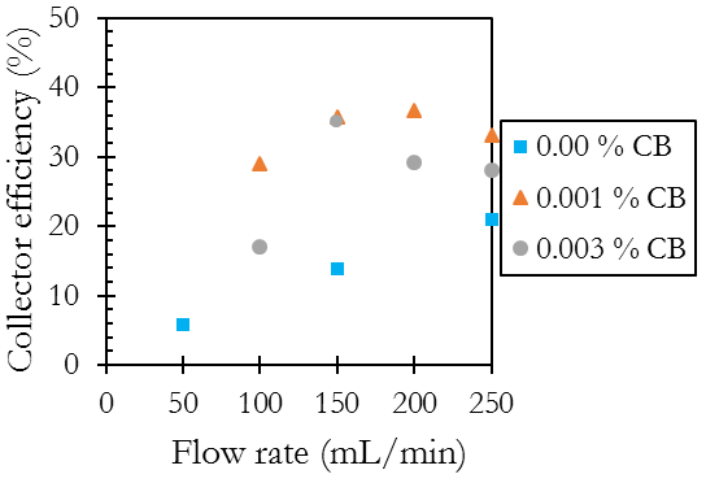

Figure 4.26: Flow rate's effect on collector efficiency.

From Figure 4.26 it can be seen that the three fluids tested show different responses to the varying flow rate. In the nature of the experiments, a significant margin of error is expected because of the dependence on different measurement values used in the calculation of the efficiency (e.g. the solar irradiation levels, the percentage losses in the optical system and the temperature measurements). For the 0.003 vol % carbon black solution it shows a peak efficiency at a flow rate of 150 mL/min after which the efficiency decreases by 6 %. It is possible that this peak is a manifestation of the error margin in the measurements. However, it is also possible that there is a degree of contribution by the, as previously discussed, absorption-flow rate relationship. If this relationship is present, it could explain the reduction in efficiency at the higher flow rates. At the higher flow rates, the extinction properties of the carbon black nanofluid would then be increased, resulting in more solar irradiation being absorbed closer to the surface of the collector and thereby increasing the convective losses from the collector. However, taking into account the graph for the outlet temperatures in Figure 4.25, the lower outlet temperature and the related reduced convective losses explain why

the higher flow rates are more efficient than the lower flow rates with a higher outlet temperature. Therefore, even if there is an absorption-flow rate relationship present in the data, it is not visible from these results as the reduced convective losses will dominate the change in efficiency due to flow rate. The 0.001 vol % carbon black nanofluid shows an increase in efficiency up to 150 mL/min after which it remains fairly consistent up until 250 mL/min where there is a 3 % drop. Similarly to the 0.003 vol % carbon black nanofluid, this result is inside the error margin that can be expected and therefore it is difficult to draw conclusions from the results. The salt water results, however, show an interesting phenomenon where the efficiency is definitely improved by higher flow rates. It can also be seen from the outlet temperature in Figure 4.25 that there is not a significant difference between the outlet temperatures at the different flow rates that would lead to a significant reduction in convective losses from the collector.

The distinct difference between the efficiencies of the single-pane vs double-pane collectors, seen in the previous section, supports the findings that the increased efficiency of the collector due to the flow rate, is influenced primarily by the decrease in outlet temperature that leads to a reduction in the convective losses from the collector. This reduction in convective losses however, does not explain the increase in efficiency with flow rate for the salt water. This supports the hypothesis that there is possibly an increase in absorption efficiency due to flow rate.

4.10.5. Nanofluid comparison

From Table 4.3 it can be seen that salt water as base fluid has a collector efficiency of 23 %. This makes sense when it is considered that water is a very good absorber of the infrared fraction of the incoming solar radiation (wavelengths above 1100 nm) that makes up approximately 30 % of the solar radiation spectrum

(Taylor et al., 2011a). This efficiency for the base fluid also corresponds with the results from (Taylor et al., 2011b) that found it to be 28 % for a highly transitive thermal oil.

Table 4.3: Collector and system efficiency for different concentration carbon black nanofluids.

Carbon black concentration (vol %)	Collector efficiency (%)	System efficiency (%)
0.00	23	11
0.0005	37	18
0.001	46	22
0.003	36	17
0.005	36	17

An immediate increase in the efficiency is seen for all the carbon black nanofluid concentrations. This is because the rest of the solar spectrum (below 1100 nm) is primarily absorbed by the carbon black nanoparticles. The system efficiency results display a similar dependence on carbon black concentration as the heating rate experiments did. The 0.0005 vol % carbon black nanofluid, although it does not absorb all of the concentrated irradiation, has almost the same efficiency as the higher 0.003 vol % and 0.005 vol % carbon black nanofluids. The higher concentration nanofluids, as seen from the heating rates as well as the efficiency comparison experiments, absorbs the irradiation closer to the surface of the collector, not allowing bulk fluid heating and results in increased convective losses from the system. As expected, the 0.001 vol % carbon black nanofluid showed the highest efficiency at 46 %, relating to a 23 % improvement in efficiency compared to that of the base fluid. This maximum achieved collector efficiency is not noteworthy. The result however, is a reflection on the collector flow cell design and amount of energy losses from the collector, not on the carbon black

nanofluid's absorption efficiency. Indicative of the benefit of utilising a nanofluid, is the increase in collector efficiency when using a nanofluid compared to that of the base fluid alone. The 23 % improvement in efficiency to that of the base fluid inside a non-ideal collector design shows promise for future work when an ideal collector is designed and implemented. But even at an excellent collector efficiency being possible in an ideal collector, the total system efficiency is still limited by the high optical losses in the concentrating steps. Therefore, for the system to possibly be viable in the future, it is necessary to reduce the optical losses in the concentrating steps. This can be done by using better quality optical materials.

5. Conclusion

Carbon black nanofluids in a base fluid of 35 g/L salt water, were produced by first coating the carbon black nanoparticles with a non-ionic surfactant, TWEEN-20, in a mass ratio of 1:2 carbon black to surfactant. The salt water was added to the coated nanoparticles and sonicated for 60 minutes. The nanofluid had an average hydrodynamic diameter of 250 nm across all the analysed carbon black concentration nanofluids. Stable carbon black nanofluids were produced at very low concentrations of less than 1 vol %. It was found that the carbon black concentration influences the stability of the colloidal suspension. The 0.0005 vol % carbon black nanofluid was visibly stable for 8 days, while the higher concentration nanofluids (below 0.01 vol %) had a visible stability of over 31 days. The carbon black concentration nanofluids above 0.01 vol % showed a much longer stability, with the 0.05 vol % carbon black nanofluid showing a visible stability of over 9 months. This increased stability at increased carbon black concentrations is either firstly because of the increased electrostatic forces between the particles when the distance between the particles is reduced, that electrostatically stabilises the nanofluid in a similar fashion as that the surfactant stabilises the colloidal suspension; or alternatively, because of the fraction of particles unwetted by the added surfactant prior to being dispersed in the nanofluid settling out, but only being visible in the lower concentration nanofluids because at 0.05 vol % carbon black the new 'effective' concentration after the settling occurred is still above the concentration where the settling will be visible. It can also be a combination of the two occurring phenomena.

It was found that at extremely low concentrations, at and below 0.001 vol % carbon black, the optical absorption properties showed a linear relationship between path length and absorption. Above concentrations of 0.001 vol % the relationship was highly exponential. The extinction coefficients in the visible light

region showed a linear decrease when the wavelength increased, relating to increased absorption of lower wavelength light. Carbon black nanofluids however, still showed excellent absorption properties across the entire solar radiation spectrum. From the photothermal property experiments, it was found that for a non-concentrating situation, there was not a big difference in the photothermal properties for the different carbon black concentrations. However, the lower concentrations, below 0.005 vol %, showed slightly better performance because the solar irradiation penetrated into the bulk fluid and was not absorbed at the surface, leading to higher convective energy losses from the surface, as was the case for the higher concentration nanofluids.

The heating rates of the nanofluids under concentrated solar irradiation showed that the carbon black concentration in the nanofluid played a critical role in the efficiency of the collector, as the higher concentration nanofluids showed a lower efficiency than the lower concentration nanofluids. The most efficient carbon black concentration, for a 2.5 cm deep collector, was found as 0.001 vol % carbon black, which showed a 42 % improvement in the heating rate compared to that of salt water. A reduced heating rate compared to that of salt water was seen for the 0.01 vol % carbon black nanofluid. This supports the findings from the photothermal experiments, that the position of solar absorption, allowing the solar irradiation to penetrate the bulk fluid, is critical in reducing the convective losses from the system and thereby resulting in a more efficient system.

It was found that a 5 cm deep collector, with an increased absorbing path length, does not show a benefit over the 2.5 cm deep collector for any of the carbon black nanofluids, it only benefited the salt water. A double-pane polycarbonate lid showed a significant influence on the collector's efficiency, confirming that convective losses from the system play a big role in the low collector efficiencies present. No clear conclusions could be drawn regarding the effect that flow rate

has on efficiency from these experiments, as the collector efficiency results were dominated by the decrease in convective losses because of a lower outlet temperature at higher flow rates.

All of the nanofluids in the flow cell experiments showed an increased efficiency compared to that of salt water. The most efficient carbon black concentration nanofluid was found to be 0.001 vol % with a 46 % collector efficiency, 23 % higher than the salt water. This low collector efficiency is contributed to high losses from the collector and a non-ideal collector design. The overall system efficiency was only 22 % for the 0.001 vol % carbon black nanofluid. This is a result of the high optical losses in the concentrating steps which were between 50 % and 70 %, depending on the cleanliness of the optical surfaces.

6. Recommendations

This report was the first step towards a very big goal of CSP driven desalination. As such there is still a lot of work to be done to fully understand the system. The recommendations for the work to follow can be categorised into two parts. The first of which is to find explanations to some behaviours of the nanofluid witnessed in the experiments. It is necessary that further tests be done to quantify the stability of the carbon black nanofluids and thereby find a better understanding of the carbon black concentration vs stability relationship and why the higher carbon black concentrations showed a higher stability. It is also further recommended that an experimental setup is designed to investigate the hypothesis that there exists an increase in absorption at higher flow rates for nanofluids. This should be done in a way that the losses from the system do not overshadow the results. A detailed CFD analysis of the collector and fluid flow will go a far way to better understand the behaviour that was witnessed.

The second part of the recommendation of future work entails the next step in the project and that is the desalination system itself. It is necessary to fully quantify the collector energy losses that, not only a fluid efficiency can be calculated, but a better collector can be designed that will show the improved efficiency expected from the system. This will be essential for the next step in the project which is to design and build the flash desalination system around the collector and compare its efficiency and desalinated water production rate.

7. References

ASTM 2006. E490 - 00a(2006) Standard Solar Constant and Zero Air Mass Solar Spectral Irradiance Tables.

ASTM 2012. G173-03(2012) Standard Tables for Reference Solar Spectral Irradiances: Direct Normal and Hemispherical on 37° Tilted Surface. West Conshohocken, PA: ASTM International.

BROOKS, M. J., DU CLOU, S., VAN NIEKERK, W. L., GAUCHÉ, P., LEONARD, C., MOUZOURIS, M. J., MEYER, R., VAN DER WESTHUIZEN, N., VAN DYK, E. E. & VORSTER, F. J. 2015. SAURAN: A new resource for solar radiometric data in Southern Africa. *Journal of Energy in Southern Africa,* 26**,** 2-10.

CHOI, C., YOO, H. S. & OH, J. M. 2008. Preparation and heat transfer properties of nanoparticle-in-transformer oil dispersions as advanced energy-efficient coolants. *Current Applied Physics,* 8**,** 710-712.

DEKKER, J., NTHONTHO, M., CHOWDHURY, S. & CHOWDHURY, S. P. 2012. Investigating the effects of solar modelling using different solar irradiation data sets and sources within South Africa. *Solar Energy,* 86**,** 2354-2365.

DWAF 1996. South African Water Quality Guidelines (second edition), Volume 2: Recreational Use.

FENDLER, J. 2001. Colloid chemical approach to nanotechnology. *Korean Journal of Chemical Engineering,* 18**,** 1-13.

GHADIMI, A., SAIDUR, R. & METSELAAR, H. S. C. 2011. A review of nanofluid stability properties and characterization in stationary conditions. *International Journal of Heat and Mass Transfer,* 54**,** 4051-4068.

GHAFFOUR, N., BUNDSCHUH, J., MAHMOUDI, H. & GOOSEN, M. F. A. 2015. Renewable energy-driven desalination technologies: A comprehensive review on challenges and potential applications of integrated systems. *Desalination,* 356**,** 94-114.

GOUDARZI, K., NEJATI, F., SHOJAEIZADEH, E. & ASADI YOUSEF-ABAD, S. K. 2015. Experimental study on the effect of pH variation of nanofluids on the thermal efficiency of a solar collector with helical tube. *Experimental Thermal and Fluid Science,* 60**,** 20-27.

GUPTA, H., AGRAWAL, G. & MATHUR, J. 2012. An overview of Nanofluids: A new media towards green environment. *International Journal of environmental sciences,* 3**,** 433-440.

HAN, D., MENG, Z., WU, D., ZHANG, C. & ZHU, H. 2011. Thermal properties of carbon black aqueous nanofluids for solar absorption. *Nanoscale Research Letters,* 6**,** 1-7.

HORDY, N., RABILLOUD, D., MEUNIER, J.-L. & COULOMBE, S. 2014. High temperature and long-term stability of carbon nanotube nanofluids for direct absorption solar thermal collectors. *Solar Energy,* 105**,** 82-90.

HWANG, Y., LEE, J.-K., LEE, J.-K., JEONG, Y.-M., CHEONG, S.-I., AHN, Y.-C. & KIM, S. H. 2008. Production and dispersion stability of nanoparticles in nanofluids. *Powder Technology,* 186**,** 145-153.

KALOGIROU, S. A. 2004. Solar thermal collectors and applications. *Progress in Energy and Combustion Science,* 30**,** 231-295.

KASAEIAN, A., ESHGHI, A. T. & SAMETI, M. 2015. A review on the applications of nanofluids in solar energy systems. *Renewable and Sustainable Energy Reviews,* 43**,** 584-598.

LADJEVARDI, S. M., ASNAGHI, A., IZADKHAST, P. S. & KASHANI, A. H. 2013. Applicability of graphite nanofluids in direct solar energy absorption. *Solar Energy,* 94**,** 327-334.

LE ROUX, W. G. 2016. Optimum tilt and azimuth angles for fixed solar collectors in South Africa using measured data. *Renewable Energy,* 96, Part A**,** 603-612.

LI, C., GOSWAMI, Y. & STEFANAKOS, E. 2013. Solar assisted sea water desalination: A review. *Renewable and Sustainable Energy Reviews,* 19**,** 136-163.

LI, Y., ZHOU, J. E., TUNG, S., SCHNEIDER, E. & XI, S. 2009. A review on development of nanofluid preparation and characterization. *Powder Technology,* 196**,** 89-101.

LIU, J., YE, Z., ZHANG, L., FANG, X. & ZHANG, Z. 2015. A combined numerical and experimental study on graphene/ionic liquid nanofluid based direct absorption solar collector. *Solar Energy Materials and Solar Cells,* 136**,** 177-186.

MERCATELLI, L., SANI, E., FONTANI, D., ZACCANTI, G., MARTELLI, F. & DI NINNI, P. 2011. *Scattering and absorption properties of carbon nanohorn-based nanofluids for solar energy applications*.

MORADI, A., SANI, E., SIMONETTI, M., FRANCINI, F., CHIAVAZZO, E. & ASINARI, P. 2015. Carbon-Nanohorn Based Nanofluids for a Direct Absorption Solar Collector for Civil Application. *Journal of Nanoscience and Nanotechnology,* 15**,** 3488-3495.

NEUMANN, O., URBAN, A. S., DAY, J., LAL, S., NORDLANDER, P. & HALAS, N. J. 2013. Solar Vapor Generation Enabled by Nanoparticles. *ACS Nano,* 7**,** 42-49.

NORMAN, D. T. 2014. *Rubber grade carbon blacks* [Online]. Continental Carbon. Available: http://www.continentalcarbon.com/pdfs/What_Is_Carbon_Black.pdf [Accessed 27 October 2015].

OGUNJOBI, K. O., KIM, Y. J. & HE, Z. 2004. Influence of the total atmospheric optical depth and cloud cover on solar irradiance components. *Atmospheric Research,* 70**,** 209-227.

OTANICAR, T., PHELAN, P. E., PRASHER, R. S., ROSENGARTEN, G. & TAYLOR, R. A. 2010a. Nanofluid-based direct absorption solar collector. *J Renewable and Sustainable Energy,* 2.

OTANICAR, T. P., PHELAN, P. E. & GOLDEN, J. S. 2009. Optical properties of liquids for direct absorption solar thermal energy systems. *Solar Energy,* 83**,** 969-977.

OTANICAR, T. P., PHELAN, P. E., PRASHER, R. S., ROSENGARTEN, G. & TAYLOR, R. A. 2010b. Nanofluid-based direct absorption solar collector. *Journal of Renewable and Sustainable Energy,* 2**,** 033102.

PAGURA, C., BARISON, S., BATTISTON, S. & SCHIAVON, M. 2010. Synthesis and characterization of single wall carbon nanohorns produced by direct vaporization of graphite. *Proceeding of TechConnect World. Volume,* 1.

PARADISE, M. & GOSWAMI, T. 2007. Carbon nanotubes – Production and industrial applications. *Materials & Design,* 28**,** 1477-1489.

PIERSON, H. O. 1993. 10 - Natural Graphite, Graphite Powders, Particles, and Compounds. *In:* PIERSON, H. O. (ed.) *Handbook of Carbon, Graphite, Diamonds and Fullerenes.* Oxford: William Andrew Publishing.

RASTOGI, R., KAUSHAL, R., TRIPATHI, S. K., SHARMA, A. L., KAUR, I. & BHARADWAJ, L. M. 2008. Comparative study of carbon nanotube dispersion using surfactants. *Journal of Colloid and Interface Science,* 328**,** 421-428.

SANI, E., MERCATELLI, L., BARISON, S., PAGURA, C., AGRESTI, F., COLLA, L. & SANSONI, P. 2011. Potential of carbon nanohorn-based suspensions for solar thermal collectors. *Solar Energy Materials and Solar Cells,* 95**,** 2994-3000.

SAROHA, S., MITTAL, T., MODI, P. J., BHALLA, V., KHULLAR, V., TYAGI, H., TAYLOR, R. A. & OTANICAR, T. P. 2015. Theoretical Analysis and Testing of Nanofluids-Based Solar Photovoltaic/Thermal Hybrid Collector. *Journal of Heat Transfer,* 137**,** 091015-091015.

SHARON, H. & REDDY, K. S. 2015. A review of solar energy driven desalination technologies. *Renewable and Sustainable Energy Reviews,* 41**,** 1080-1118.

SKOOG, D. A., CROUCH, S. R. & HOLLER, F. J. 2007. *Principles of instrumental analysis,* Belmont, CA, Thomson Brooks/Cole.

SUMAN, S., KHAN, M. K. & PATHAK, M. 2015. Performance enhancement of solar collectors—A review. *Renewable and Sustainable Energy Reviews,* 49**,** 192-210.

TAYLOR, R., COULOMBE, S., OTANICAR, T., PHELAN, P., GUNAWAN, A., LV, W., ROSENGARTEN, G., PRASHER, R. & TYAGI, H. 2013. Small particles, big impacts: A review of the diverse applications of nanofluids. *Journal of Applied Physics,* 113**,** 011301.

TAYLOR, R. A., PHELAN, P. E., ADRIAN, R. J., GUNAWAN, A. & OTANICAR, T. P. 2012. Characterization of light-induced, volumetric steam generation in nanofluids. *International Journal of Thermal Sciences,* 56**,** 1-11.

TAYLOR, R. A., PHELAN, P. E., OTANICAR, T. P., ADRIAN, R. & PRASHER, R. 2011a. Nanofluid optical property characterization: towards efficient direct absorption solar collectors. *Nanoscale Research Letters,* 6**,** 1-11.

TAYLOR, R. A., PHELAN, P. E., OTANICAR, T. P., WALKER, C. A., NGUYEN, M., TRIMBLE, S. & PRASHER, R. 2011b. Applicability of nanofluids in high flux solar collectors. *Journal of Renewable and Sustainable Energy,* 3**,** 023104.

TYAGI, H., PHELAN, P. & PRASHER, R. 2009. Predicted Efficiency of a Low-Temperature Nanofluid-Based Direct Absorption Solar Collector. *Journal of Solar Energy Engineering,* 131**,** 041004-041004.

VANDER WAL, R. L., MOZES, S. D. & PUSHKAREV, V. 2009. Nanocarbon nanofluids: morphology and nanostructure comparisons. *Nanotechnology,* 20**,** 105702.

WAGNER, T. R., HOUF, W. G. & INCROPERA, F. P. 1980. Radiative property measurements for india ink suspensions of varying concentration. *Solar Energy,* 25**,** 549-554.

XIE, H., LEE, H., YOUN, W. & CHOI, M. 2003. Nanofluids containing multiwalled carbon nanotubes and their enhanced thermal conductivities. *Journal of Applied Physics,* 94**,** 4967-4971.

YOUSEFI, T., VEISY, F., SHOJAEIZADEH, E. & ZINADINI, S. 2012. An experimental investigation on the effect of MWCNT-H2O nanofluid on the efficiency of flat-plate solar collectors. *Experimental Thermal and Fluid Science,* 39**,** 207-212.

YU, W. & XIE, H. 2012. A Review on Nanofluids: Preparation, Stability Mechanisms, and Applications. *Journal of Nanomaterials,* 2012**,** 17.

ZARZA, E. & ROMERO-ALVAREZ, M. 2007. Concentrating Solar Thermal Power. *Handbook of Energy Efficiency and Renewable Energy*. CRC Press.

ZHANG, L., LIU, J., HE, G., YE, Z., FANG, X. & ZHANG, Z. 2014. Radiative properties of ionic liquid-based nanofluids for medium-to-high-temperature direct absorption solar collectors. *Solar Energy Materials and Solar Cells,* 130**,** 521-528.